



Fig. 11. Schematic representation of possible orientation of PMPC brushes grown from nanopores having different graft density.

densely grafted PMPC obtained under the same polymerization condition which is 0.46 chains/nm^2 . This can be explained from the fact that the graft density of the initiator was intentionally kept low in order to avoid a complete filling of the initiator and leave some space for the polymer brush to aggregate in the nanopores. In other words, the number of grafted chains for the high graft density (0.46 chains/nm^2) should be approximately 9–23 times higher than that for the low graft density ($0.02\text{--}0.05 \text{ chains/nm}^2$) (see Fig. 11).

The surfaces whose nanopores were almost completely covered with PMPC brushes were quite smooth and the protrusions simultaneously diminished, as can be observed in Figs. 10c and 10d. Such behavior might stem from the fact that PMPC brushes were dense enough to be able to fill the nanopores and to eliminate the valley-and-hill features on the surface. The disappearance of the protrusions may be facilitated by two possible actions of polymer brushes previously addressed. The first action involves the polymer chains being forced to stretch away from the surface and thus covering the nanopores while the other involves the folding of polymer chains over the tris(TMS) layer. This latter action should be favorable only when the polymer chains are sufficiently long. The behavior of PMPC brushes is schematically displayed in Fig. 11.

Since the density of PMPC brushes in nanopores is the key to the ability to visualize the polymer distribution, the second alternative route was then performed by varying the %tris(TMS) coverage but fixing the graft density of the initiator at a low value by using a short reaction time (24 h) between the silicon-supported mixed tris(TMS)/silanol monolayers and the silane compound. These experiments were designed in order to make sure that the residual silanols in nanopores were not completely replaced by the α -bromoisobutyrate groups and that there was some space between the grafted PMPC brushes and the surrounding tris(TMS). After the formation of polymer brushes, there should be some space for PMPC brushes to aggregate inside the nanopores. AFM images of the silicon-supported mixed tris(TMS)/PMPC brushes prepared by this approach using a 1 h polymerization time are illustrated in Fig. 12. The size of protrusions obviously reflected the size of nanopores, which should be inversely proportional to %tris(TMS) coverage. The higher the %tris(TMS) coverage, the smaller the protrusions.

A comparative investigation has been conducted on the system of the silicon-supported mixed tris(TMS)/Pt-BMA brushes. Fig. 13 shows AFM images of the silicon-supported mixed tris(TMS)/Pt-BMA brushes having 82% tris(TMS) coverage. Pt-BMA brushes were grown for 1 h from the silicon-supported mixed tris(TMS)/ α -bromoisobutyrate having different graft densities of α -bromoisobutyrate groups. Conducting the reaction between the silicon-supported mixed tris(TMS)/silanol monolayers and silane compound having

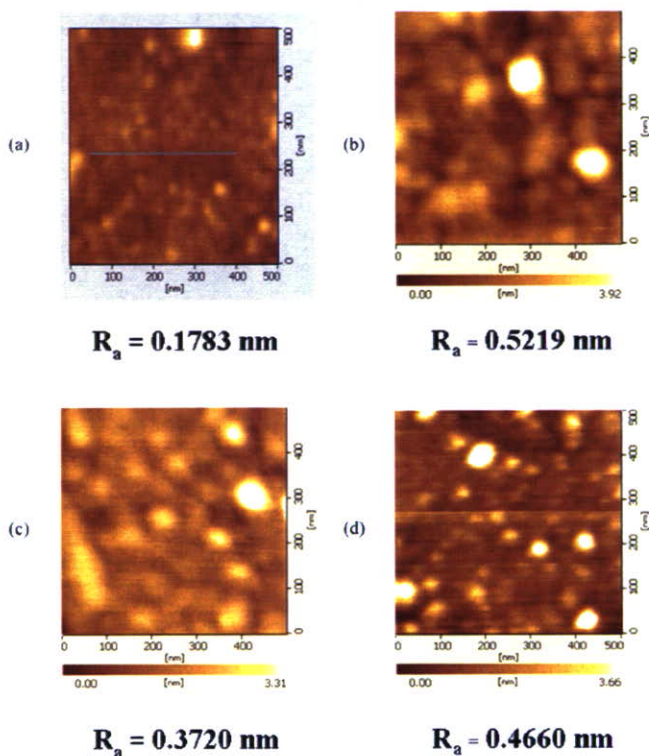


Fig. 12. AFM images of the silicon-supported mixed tris(TMS)/PMPC brushes using grafting time of initiator as 24 h and varied % tris(TMS) coverage: (a) 0, (b) 51, (c) 66, and (d) 82%.

end-functionalized α -bromoisobutyrate groups for 24 and 96 h yielded a low and high graft density of α -bromoisobutyrate groups, respectively. Even though both surfaces (Figs. 13a and 13b) have different graft densities of Pt-BMA brushes, their surface topographies are indistinguishable and relatively smooth in texture. The surfaces became rougher when the polymerization time was extended from 1 to 5 h without affecting surface topographies (Figs. 13c and 13d). Unlike PMPC brushes, Pt-BMA brushes are hydrophobic. Therefore, they should be quite miscible with tris(TMS). In fact, this speculation can be confirmed by the contact angle data shown in Fig. 5. The mixed tris(TMS)/Pt-BMA brush system thereby did not exhibit nanoscopic phase separation although the surface graft density of Pt-BMA brushes was low. These results also imply that self-aggregation of PMPC brushes in nanopores, which leads to protrusions, is truly a consequence of phase incompatibility between hydrophilic PMPC brushes and hydrophobic tris(TMS). Once again, it should be highlighted that such nanoscopic phase separation was noticeable when the graft density of PMPC brushes was low. This observation is, however, in contrast to the previous work reported by Stafford et al. [27].

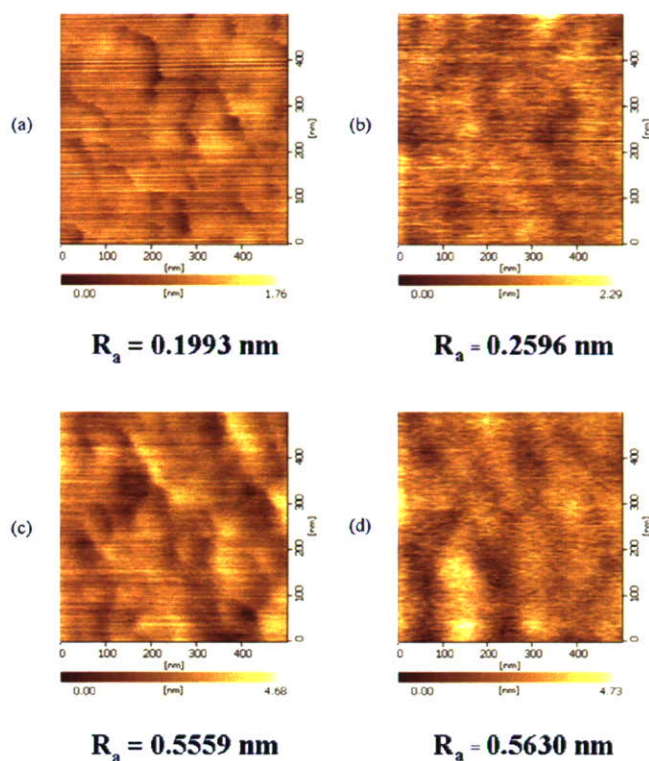


Fig. 13. AFM images of the silicon-supported mixed 82% tris(TMS)/Pt-BMA brushes, controlling the grafting time of initiator (t_i) and polymerization time (t_p): (a) $t_i = 24$ h, $t_p = 1$ h, (b) $t_i = 96$ h, $t_p = 1$ h, (c) $t_i = 24$ h, $t_p = 5$ h, and (d) $t_i = 96$ h, $t_p = 5$ h.

Despite the hydrophobicity of polystyrene ($\theta_A/\theta_R = 95^\circ/79^\circ$), the nanoscopic distribution of polystyrene aggregates was observed after the adsorption of carboxyl-terminated polystyrene on the nanoporous tris(TMS)/silanol monolayers. The dimension of aggregates corresponded very well with the %tris(TMS) coverage. We believe the following reasons account for such difference. As opposed to our “grafting from” approach, the “grafting to” approach, used in their study, should suffer an entropic barrier due to crowding of initial grafting polymer chains that prevent further insertion of polymer onto the surface. As a result, the graft density should be extremely low (lower than our Pt-BMA brushes), especially when the “grafting to” was done on the nanoporous surface. Based on their calculation, as few as one polystyrene chain was grafted in the nanopore of the surface having relatively high tris(TMS) coverage. The coil-like conformation should thus be more favorable than the extended one, leading to the aggregation of the end-grafted polystyrene regardless of its comparable hydrophobicity with the tris (TMS).

3.5. Anti-fouling characteristics of PMPC brushes in nanopores

As a biocompatible polymer, PMPC is well recognized for its anti-fouling characteristic, meaning it resists non-specific interactions with plasma proteins and cells. One way to test the effect of the nanoscopic spatial distribution of PMPC

brushes on the surface property is to determine the interactions between the silicon-supported mixed tris(TMS)/PMPC brushes having different %tris(TMS) coverage with plasma proteins. The protein adsorption data are summarized in Table 5. Due to the hydrophilic nature of the silicon substrate, the amount of protein adsorption was quite low. The amount of adsorbed protein slightly increased on a more hydrophobic silicon-supported α -bromoisobutyrate monolayer. Even though the amount of plasma protein adsorbed on the surfaces having PMPC brushes was lower than that on the surface grafted with α -bromoisobutyrate, the difference was not that significant considering the more hydrophilic nature of PMPC in comparison with the surface covered with an α -bromoisobutyrate monolayer. In order to verify that the reduction of protein adsorption was really due to the presence of PMPC brushes, Pt-BMA was chosen as a positive control. The fact that Pt-BMA brushes adsorbed a greater amount of protein as opposed to PMPC brushes helped confirm the above interpretation.

The amount of protein adsorbed on the surface having PMPC brushes was almost independent of the thickness of polymer brushes, implying that PMPC brushes being as thin as ~ 1 nm were sufficient to obtain the protein-resistance property. Apparently, the coverage of tris(TMS) played a significant role in controlling protein adsorption. The higher the content of tris(TMS) or the lower the graft density of PMPC brushes on the surface, the higher the quantity of the adsorbed protein. Unlike the silicon-supported PMPC brushes, the response to plasma proteins of the silicon-supported mixed tris(TMS)/PMPC brushes depended upon the thickness of polymer brushes. Considering the series of silicon-supported mixed 66% tris(TMS)/PMPC brushes, it seems that the longer polymer brushes were capable of repelling plasma protein despite their relatively low graft density or high %tris(TMS) coverage.

This outcome is in good agreement with the hypothesis previously proposed based on topographic evidence obtained from AFM analysis. It was postulated that the stretching of long polymer chains is thermodynamically unfavorable so the polymer chains tend to fold over the tris(TMS) monolayer. The lower receding contact angle as a function of polymer thickness can be an indication of PMPC brushes dominating at polymer/water interfaces or under hydrated conditions. As a result, the coverage of PMPC brushes is no longer directly correlated with %tris(TMS). In other words, the protein resistance is no longer dictated by %tris(TMS) but rather by the thickness of PMPC brushes instead.

In the case of homogeneously and densely grafted PMPC brushes grown from the silicon-supported α -bromoisobutyrate monolayer, the protein adsorption does not depend on the thickness of polymer brushes as long as the surface is fully covered by the polymer brushes. The extremely thin layer of polymer brushes is certainly enough for generating a non-fouling surface. On the other hand, the thickness and the graft density of polymer brushes become important parameters in controlling protein adsorption on heterogeneously and loosely grafted PMPC brushes grown from the silicon-supported tris(TMS) α -bromoisobutyrate monolayer. When polymer brushes are quite short, the polymer chains are forced to stretch out or aggregate

Table 5
The amount of plasma protein adsorbed on various silicon substrates

Surface	Thickness of polymer brushes (nm)	Water contact angle (θ_A/θ_R)	Amount of protein adsorbed ($\mu\text{g}/\text{cm}^2$)
Silicon oxide	–	$\sim 0^\circ$	0.16 ± 0.06
Silicon-supported α -bromoisobutyrate monolayer	–	$71^\circ/62^\circ$	0.33 ± 0.15
Silicon-supported PMPC brushes	1.0	$23^\circ/0^\circ$	0.23 ± 0.05
	2.6	$22^\circ/0^\circ$	0.20 ± 0.03
	6.4	$20^\circ/0^\circ$	0.17 ± 0.02
Silicon-supported Pt-BMA brushes	1.8	$92^\circ/72^\circ$	5.24 ± 0.30
	3.0	$94^\circ/77^\circ$	6.20 ± 0.20
Silicon-supported mixed 66% tris(TMS)/PMPC brushes	2.6	$56^\circ/30^\circ$	1.70 ± 0.17
	3.0	$54^\circ/27^\circ$	0.62 ± 0.05
	4.3	$54^\circ/20^\circ$	40.07 ± 0.03
Silicon-supported mixed 75% tris(TMS)/PMPC brushes	2.3	$63^\circ/31^\circ$	2.71 ± 0.09
Silicon-supported mixed 82% tris(TMS)/PMPC brushes	1.8	$70^\circ/40^\circ$	3.92 ± 0.27

in the nanopores surrounded by tris(TMS), so the protein adsorption varies as a function of %tris(TMS) or the graft density of PMPC brushes. In contrast, when the polymer brushes are so long that they can fold and partly cover tris(TMS), the protein adsorption no longer relies on %tris(TMS), but is mainly influenced by the length or the thickness of the polymer brushes. Our results are in good agreement with the data previously reported by Feng et al. [38]. They have observed that PMPC chains were very effective in preventing protein adsorption even with the short chain lengths (low thickness) at the high graft density. They have therefore concluded that graft density is more important than the chain length for preventing protein adsorption.

4. Conclusions

The incomplete reaction between the sluggish tris(TMSCI) and silicon oxide surface allowed silicon-supported mixed tris(TMS)/silanol monolayers having a range of tris(TMS) coverage to be formed. Nanoscale holes (nanopores) in tris(TMS) monolayers containing unreacted silanol groups of silicon-supported mixed tris(TMS)/silanol monolayers further reacted with silane compounds having end-functionalized α -bromoisobutyrate and yielded silicon-supported mixed tris(TMS)/ α -bromoisobutyrate monolayers. PMPC brushes grew faster from surface-immobilized α -bromoisobutyrate initiators having hexyl (n_6) and decyl (n_{10}) as alkyl spacers in comparison with propyl (n_3) as an alkyl spacer. The better mobility and the longer alkyl spacers of n_6 and n_{10} allowed them to overcome the steric hindrance of the surrounding tris(TMS) and reach monomers more efficiently than n_3 .

The nanoscopic distribution of PMPC brushes, which appeared as protrusions having a diameter of less than 100 nm, was only visualized when the graft density of PMPC brushes in the nanopores was not too high. Under such circumstances, the size of protrusions depended upon both the %tris(TMS) coverage as well as the graft density of PMPC brushes itself in the nanopores. In the case of a high graft density of PMPC brushes

in the nanopores, the surfaces became quite smooth due to the polymer chains being forced to stretch away from the surface, thus covering the nanopores, and the folding of polymer chains over the tris(TMS) layer when the polymer chains are sufficiently long. Unlike PMPC brushes, Pt-BMA brushes are hydrophobic so they should be quite compatible with tris(TMS). The mixed tris(TMS)/Pt-BMA brush system thereby did not exhibit nanoscopic phase separation although the graft density of Pt-BMA brushes in the nanopores was quite low. These results also implied that self-aggregation of PMPC brushes in the nanopores was truly a consequence of phase incompatibility between hydrophilic PMPC brushes and hydrophobic tris(TMS). The protein adsorption studies have demonstrated that the anti-fouling characteristic, a key surface property of PMPC brushes, is influenced by the percentage of tris(TMS) as well as the chain length of the polymer brushes.

Acknowledgments

This research is supported by the Thailand Research Fund (TRG4580049), a TJTTP-JBIC project (under the Center for Bioactive Compounds, Chulalongkorn University) and a graduate research grant for Mayuree Srinanthakul from Chulalongkorn University. The authors are grateful to the Capability Building Unit for Nanoscience and Nanotechnology, Mahidol University and the Electronic Research Center, Faculty of Engineering, King Mongkut's Institute of Technology, Ladkrabang for providing Atomic Force Microscopy and Ellipsometry facilities, respectively. Appreciation is also extended to the National Metal and Materials Technology Center (MTEC) for providing the contact angle goniometer.

References

- [1] S.T. Milner, Science 251 (1991) 905.
- [2] A. Halperin, M. Tirrell, T.P. Lodge, Adv. Polym. Sci. 100 (1992) 31.
- [3] B. Zhao, W.J. Brittain, Prog. Polym. Sci. 25 (2000) 677.
- [4] Y. Ito, Y. Ochiai, Y.S. Park, Y. Imanishi, J. Am. Chem. Soc. 119 (1997) 1619.

- [5] Y.S. Park, Y. Ito, Y. Imanishi, *Macromolecules* 31 (1998) 2606.
- [6] O. Prucker, J. R uhe, *Macromolecules* 31 (1998) 592.
- [7] X. Huang, M.J. Wirth, *Macromolecules* 32 (1999) 1694.
- [8] K. Matyjaszewski, P.J. Miller, N. Shukla, B. Immaraporn, A. Gelman, B.B. Luokala, T.M. Siclovan, G. Kickelbick, T. Vallant, H. Hoffman, T. Pakula, *Macromolecules* 32 (1999) 8716.
- [9] J.B. Kim, M.L. Bruening, G.L. Baker, *J. Am. Chem. Soc.* 122 (2000) 7616.
- [10] B. Zhao, W.J. Brittain, *Macromolecules* 33 (2000) 8813.
- [11] M. Ejaz, K. Ohno, Y. Tsuji, T. Fukuda, *Macromolecules* 33 (2000) 2870.
- [12] T. von Werne, T.E. Patten, *J. Am. Chem. Soc.* 123 (2001) 7497.
- [13] M. Husemann, E.E. Malmstrom, M. McNamara, M. Mate, D. Mecerreyes, D.G. Benoit, J.L. Hedrick, P. Mansky, E. Huang, T.P. Russell, C.J. Hawker, *Macromolecules* 32 (1999) 1424.
- [14] H. Mori, A. B oker, G. Krausch, A.H.E. M uller, *Macromolecules* 34 (2001) 6871.
- [15] M. Khan, W.T.S. Huck, *Macromolecules* 36 (2003) 5088.
- [16] J. R uhe, *Macromol. Symp.* 126 (1998) 215.
- [17] G.P. Chen, Y. Ito, Y. Imanishi, *Macromolecules* 30 (1997) 7001.
- [18] M. Husemann, M. Morrison, D. Benoit, K.J. Frommer, C.M. Mate, W.D. Hinsberg, J.L. Hedrick, C.J. Hawker, *J. Am. Chem. Soc.* 122 (2000) 1844.
- [19] J. Aizenberg, A.J. Black, G.M. Whitesides, *Nature* 394 (1998) 868.
- [20] A.J. Black, K.E. Paul, J. Aizenberg, G.M. Whitesides, *J. Am. Chem. Soc.* 121 (1999) 8356.
- [21] M. Husemann, D. Mecerreyes, C.J. Hawker, J.L. Hedrick, R. Shah, N.L. Abbott, *Angew. Chem. Int. Ed.* 38 (1999) 647.
- [22] R.R. Shah, D. Mecerreyes, M. Husemann, I. Rees, N.L. Abbott, C.J. Hawker, J.L. Hedrick, *Macromolecules* 33 (2000) 597.
- [23] L. Yan, W.T.S. Huck, X.M. Zhao, G.M. Whitesides, *Langmuir* 15 (1999) 1208.
- [24] R.W. Zehner, L.R. Sita, *Langmuir* 15 (1999) 6139.
- [25] D. Mecerreyes, E. Huang, T. Magbitang, W. Volksen, C.J. Hawker, V.Y. Lee, R.D. Miller, J.L. Hedrick, *High Perform. Polym.* 13 (2001) S11.
- [26] A.Y. Fadeev, T.J. McCarthy, *Langmuir* 15 (1999) 7238.
- [27] C.M. Stafford, A.Y. Fadeev, T.P. Russell, T.J. McCarthy, *Langmuir* 17 (2001) 6547.
- [28] X. Jia, T.J. McCarthy, *Langmuir* 19 (2003) 2449.
- [29] J.N. Israelachvili, M.L. Gee, *Langmuir* 5 (1989) 288.
- [30] K. Ishihara, H. Oshida, Y. Endo, A. Watanabe, T. Ueda, N. Nakabayashi, *J. Biomed. Mater. Res.* 27 (1993) 1309.
- [31] K. Ishihara, H. Nomura, T. Mihara, K. Kurita, Y. Iwasaki, N. Nakabayashi, *J. Biomed. Mater. Res.* 39 (1998) 323.
- [32] Y. Iwasaki, S. Sawada, K. Ishihara, G. Khang, H.B. Lee, *Biomaterials* 23 (2002) 3897.
- [33] S. Sawada, S. Sakaki, Y. Iwasaki, N. Nakabayashi, K. Ishihara, *J. Biomed. Mater. Res. A* 64 (2003) 411.
- [34] X.Y. Chen, S.P. Armes, *Adv. Mater.* 15 (2003) 1558.
- [35] W. Feng, J. Brash, S.P. Zhu, *J. Polym. Sci. Polym. Chem.* 42 (2004) 2931.
- [36] R. Iwata, P. Suk-in, V.P. Hoven, A. Takahara, K. Akiyoshi, Y. Iwasaki, *Biomacromolecules* 5 (2004) 2308.
- [37] W. Feng, S.P. Zhu, K. Ishihara, J.L. Brash, *Langmuir* 21 (2005) 5980.
- [38] W. Feng, J.L. Brash, S.P. Zhu, *Biomaterials* 27 (2006) 847.
- [39] S. Heid, F. Effenberger, K. Bierbaum, M. Grunze, *Langmuir* 12 (1996) 2118.
- [40] M. Ejaz, Y. Tsujii, T. Fukuda, *Polymer* 42 (2001) 6811.

Selective Biorecognition and Preservation of Cell Function on Carbohydrate-Immobilized Phosphorylcholine Polymers

Yasuhiko Iwasaki,^{*,†,‡} Utae Takami,^{‡,§} Yurika Shinohara,^{‡,§} Kimio Kurita,[§] and Kazunari Akiyoshi^{‡,||}

Department of Chemistry and Materials Engineering, Faculty of Chemistry, Materials and Bioengineering, Kansai University, 3-3-35 Yamate-cho, Suita-shi, Osaka 564-8680, Japan, Institute of Biomaterials and Bioengineering and Center of Excellence Program for Frontier Research on Molecular Destruction and Reconstruction of Tooth and Bone, Tokyo Medical and Dental University, 2-3-10 Kanda-surugadai, Chiyoda-ku, Tokyo 101-0062, Japan, and Department of Materials and Applied Chemistry, College of Science and Technology, Nihon University, 1-8-14 Kanda-surugadai, Chiyoda-ku, Tokyo 101-8308, Japan

Received April 30, 2007; Revised Manuscript Received June 13, 2007

To obtain synthetic materials capable of selectively recognizing proteins and cells, and preserving their functions, biomembrane mimetic polymers having a phospholipid polar group and carbohydrate side chains were designed. Poly[2-methacryloyloxyethyl phosphorylcholine (MPC)-*co*-*n*-butyl methacrylate (BMA)-*co*-2-lactobionamidoethyl methacrylate (LAMA)] (PMBL) was synthesized and coated on substrates by solvent evaporation. Selective binding of galactose-recognized lectin, RCA₁₂₀, to a PMBL surface was investigated by measurement of surface plasmon resonance. The binding of RCA₁₂₀ to the PMBL surface was confirmed by a remarkable change in resonance angle. The apparent affinity constant of RCA₁₂₀ to PMBL3.0 (3.0 mol % LAMA unit in the feed) per LAMA unit was $2.77 \times 10^5 \text{ M}^{-1}$. When a glucose-recognized lectin, concanavalin A, was in contact with PMBL, no change in the resonance angle was observed, and any nonspecific fouling of protein on PMBL was effectively reduced. Cells of the human hepatocellular liver carcinoma cell line (HepG2) having asialoglycoprotein receptors (ASGPRs) were seeded on polymer surfaces. On poly(BMA) (PBMA), many adherent cells were observed and were well-spread with monolayer adhesion, but cell adhesion was reduced on poly(MPC-*co*-BMA) (PMB). HepG2 adhesion was observed on PMBL because the cell has ASGPRs; the number of cells adhering to the PMBL polymer surfaces increased with an increase in the density of galactose residues on the surface. In contrast, adhesion of NIH-3T3 cells to PMBL was reduced in a manner similar to that on PMB because the NIH-3T3 cells did not have ASGPRs. Cell adhesion to the PMBL surface was well-regulated by ligand–receptor interactions. Furthermore, some of the cells adhering to the PMBL surface had a spheroid form, and similarly shaped spheroids were scattered on the surface. Although poly(BMA-*co*-LAMA) (PBL) has galactose residues, the adherent cells were spread in a manner similar to those on PBMA. The MPC units in PMBL contribute to make a spheroid formation of HepG2 cells. The amount of albumin secreted from a cell was compared with the chemical structure of the substrate. The spheroid shaped cells cultured on the PMBL surface secreted much more albumin than did the spreading cells that adhered to the PBMA. In conclusion, the biomembrane mimetic carbohydrate-immobilized phosphorylcholine polymers produced a suitable surface for biorecognition and preservation of cell function.

Introduction

Control of cell adhesion and the function of synthetic polymers are important in molecular separation, biosensors, and development of biomedical materials.^{1,2} In this article, we explore the ability of biomembrane mimetic polymer surfaces to recognize specific biosubstances from their physiological conditions.

Using physicochemical and biological approaches, various surface conditions, such as a wettability gradient,³ topological patterns,^{4,5} peptide immobilization,^{6–13} and carbohydrates^{14–20} have been applied to control cell attachment. The physicochem-

ical or topological systems enable control of the surface density of adherent cells, but these surfaces cannot recognize the specific type of cell. By ligand immobilization on a synthetic surface, recognition selectivity could be improved. Arg–Gly–Asp (RGD) immobilized surfaces have been studied extensively to induce cell adhesion based on ligand–receptor interactions.^{6,11–13} While these approaches improved cell adhesion, the selectivity of RGD is limited because the RGD sequence is not unique for a specific cell. The immobilization was generally performed on conventional polymers, and nonspecific interactions occurred between the cell and the synthetic surface.

Carbohydrates are also one of the most reliable candidates as ligands immobilized on a surface because carbohydrates on a cell surface contribute to most forms of communication between living cells and their environment.¹⁶ In particular, galactose residues are preferably conjugated polymers to interact with hepatocytes, which are asialoglycoprotein receptors (ASGPRs). The ASGPR is a lectin for receptor-mediated endocytosis found at the hepatocyte cell surface, which is bound to galactose/*N*-acetylgalactosamine (GalNAc)-terminated ligands

* Corresponding author. Tel.: +81-6-6368-0090; fax: +81-6-6368-0090; e-mail: yasu.bmt@ipc.kansai-u.ac.jp.

[†] Kansai University.

[‡] Institute of Biomaterials and Bioengineering, Tokyo Medical and Dental University.

[§] Nihon University.

^{||} Center of Excellence Program for Frontier Research on Molecular Destruction and Reconstruction of Tooth and Bone, Tokyo Medical and Dental University.

Table 1. Synthetic Results and Surface Characterization of PMBL

abbreviation	molar fraction (MPC/BMA/LAMA)		M_w (10^5)	M_w/M_n	XPS elemental data (%) ^a			
	in feed ^b	in copolymer ^c			C	O	N	P
PMBL0.5	0.200/0.795/0.005	0.192/0.801/0.006	4.7	2.1	71.4 (72.8)	25.1 (23.9)	1.3 (1.7)	2.2 (1.6)
PMBL1.0	0.200/0.790/0.010	0.172/0.817/0.011	3.7	1.7	70.5 (73.2)	25.3 (23.8)	1.8 (1.6)	2.4 (1.5)
PMBL3.0	0.200/0.770/0.030	0.180/0.801/0.019	3.4	1.8	70.2 (72.5)	26.5 (24.3)	1.6 (1.7)	1.7 (1.5)
PMB	0.300/0.700/–	0.314/0.686/–	7.4	1.8	71.0 (69.7)	25.2 (25.4)	1.3 (2.4)	2.5 (2.4)
PBL1.0	–/0.990/0.010	–/0.992/0.008	2.4	1.5	– (79.4)	– (20.5)	– (0.1)	– (–)

^a Takeoff angle = 90°. Theoretical elemental data calculated from bulk concentration are in parentheses. ^b [Monomer] = 1.0 M, [AIBN] = 5 mM, temperature = 60 °C, and solvent is EtOH/DMSO. ^c Determined by phosphorus analysis and anthrone sulfuric acid method.

in a calcium-dependent manner.^{17,18} Although the ASGPR does not function physiologically as an adhesion receptor, galactose-containing polymers have been used to induce adhesion in primary hepatocytes.^{19–21} Various polymers bearing galactose residues as ligands were prepared for drug delivery²² and cellular matrices.²³ While these approaches have been quite successful, limitations remain in terms of selective recognition.²⁴ Indeed, most earlier reports did not focus on the reduction of nonspecific interactions.

We have been studying 2-methacryloyloxyethyl phosphorylcholine (MPC) polymers synthesized as biomimetics of phospholipids in a biomembrane.^{25–28} MPC polymers have a surface that resists nonspecific protein adsorption and cell adhesion (i.e., biofouling).^{29,30} Biofouling reduces the functionality of a material and can induce an unexpected bioreaction. Further, it has been shown that cells in contact with MPC polymers do not exhibit activation or an inflammatory response.^{31,32} Although nonfouling phenomena of MPC polymer surfaces have been extensively studied, carbohydrate-immobilized MPC polymers have not been synthesized for creating biorecognition surfaces.

We hypothesized that MPC polymer surfaces bearing carbohydrates might perform in the same way as biomembrane mimetic surfaces, which can interact with a specific cell and control its function. In this study, an MPC copolymer with galactose residues has been synthesized for the first time, and we present here the effectiveness of the surface in controlling cell–material interactions and preserving cell function.

Materials and Methods

Polymer Synthesis. *n*-Butyl methacrylate (BMA) was purified by conventional distillation. MPC was synthesized as previously reported.³³ 2-Lactobionamidoethyl methacrylate (LAMA) was synthesized by reacting lactobionolactone and 2-aminoethyl methacrylate hydrochloride.³⁴ Other reagents and solvents were obtained commercially in extra-pure grade and used without further purification.

Poly(MPC-*co*-BMA) (PMB), poly(BMA-*co*-LAMA) (PBL), and poly(MPC-*co*-BMA-*co*-LAMA) (PMBL) were synthesized by conventional radical polymerization using 2,2'-azobisisobutyronitrile (AIBN) as an initiator. BMA was used as a comonomer because it enables the processing of a polymer membrane. The mole fraction of the MPC and LAMA units in the polymer was determined by phosphorus analysis and the anthrone sulfate method, respectively. The number-averaged and weight-averaged molecular weights of the polymers were determined with a Tosoh gel permeation chromatography (GPC) system with a refractive index detector and size exclusion columns (Polymer Laboratories Ltd.) and MIXED-C with a poly(methyl methacrylate)

standard (PMMA, Tosoh standard sample) in CHCl₃ or CHCl₃/methanol (6:4, vol/vol). The results of polymerization are summarized in Table 1.

Preparation of Sample Plates for Cell Culture Experiments. Poly(ethylene terephthalate) (PET) plates (14 mm in diameter; Wako Pure Chemical Industries, Ltd.) were immersed in an ethanol or toluene solution of the polymer (0.5 wt %) and dried under a vapor atmosphere of the solvent at room temperature for 30 min. This procedure was repeated twice, after which the plates were dried in vacuo. The surface properties of the polymer-coated PET plates were analyzed by surface contact angle measurement (G-1, Erma) and X-ray photoelectron spectroscopy (XPS; Kratos-Shimadzu) with a magnesium anode (takeoff angle of 90°). Survey scan spectra of C_{1s}, O_{1s}, N_{1s}, and P_{2p} were taken.

Selective Binding of Lectins on Polymer Surfaces. The binding of lectins on the polymer surfaces was determined by a surface plasmon resonance (SPR; Moritex) sensor. Gold-spattered sensor chips were purchased from Moritex, and the polymers were further coated using a spin coater (ACT-220A, ACTIVE Co., Ltd.) at 4000 rpm from a 0.25 wt % solution. The running buffer for the SPR was a phosphate buffered solution (PBS; 150 mM sodium chloride, pH 7.4). Galactose-recognizing lectin (RCA₁₂₀; Vector Laboratories, Inc.) or glucose binding lectin, concanavalin A (Con A; Vector Laboratories, Inc.), was in contact with the polymer-coated sensor chips. After the lectin solution was in contact with the polymer surfaces for 10 min, the surfaces of the sensor chips were rinsed with running buffer. The change in resonance angle due to the adsorption/desorption of lectin was monitored. Apparent affinity constants per LAMA unit (K_a) and changes in maximum angle ($\Delta\theta_{\max}$) were calculated from the slope and intercepts according to Langmuir (eq 1)³⁵

$$[\text{lectin}]/\Delta\theta = [\text{lectin}]/\Delta\theta_{\max} + 1/\Delta\theta_{\max}K_a \quad (1)$$

Cell Culture Experiments. Before the cell culture experiments were performed, protein adsorption on the polymer surfaces from the culture medium was determined because cell adhesion is strongly dependent on protein adsorption. PBMA-, PMBL-, and PBL-coated PET plates were placed in contact with PBS to equilibrate their surfaces. The plates were then soaked in the culture medium (Eagle's MEM; Nissui Pharmaceutical) containing 10% fetal bovine serum (FBS) at 37 °C. The amount of adsorbed proteins on the polymer surfaces from 10% FBS was determined by the micro-BCA method.³⁶

Human hepatocellular liver carcinoma cell line (HepG2) cells and mouse fibroblasts (NIH-3T3) were purchased from RIKEN Cell Bank. The cells were maintained in a culture medium containing 10% FBS at 37 °C in a humidified atmosphere of air containing 5% CO₂. For cell maintenance, the contents of the flasks were detached by trypsin treatment. The concentration of the cells was adjusted to 2.0 × 10⁴ cells/mL. The cells (1 mL suspension) were seeded on the polymer surfaces and continuously cultured for specific periods in the CO₂

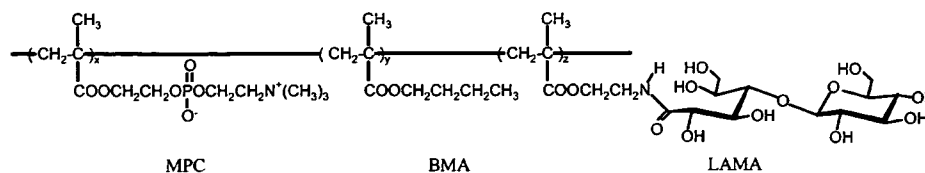


Figure 1. Structure of PMBL.

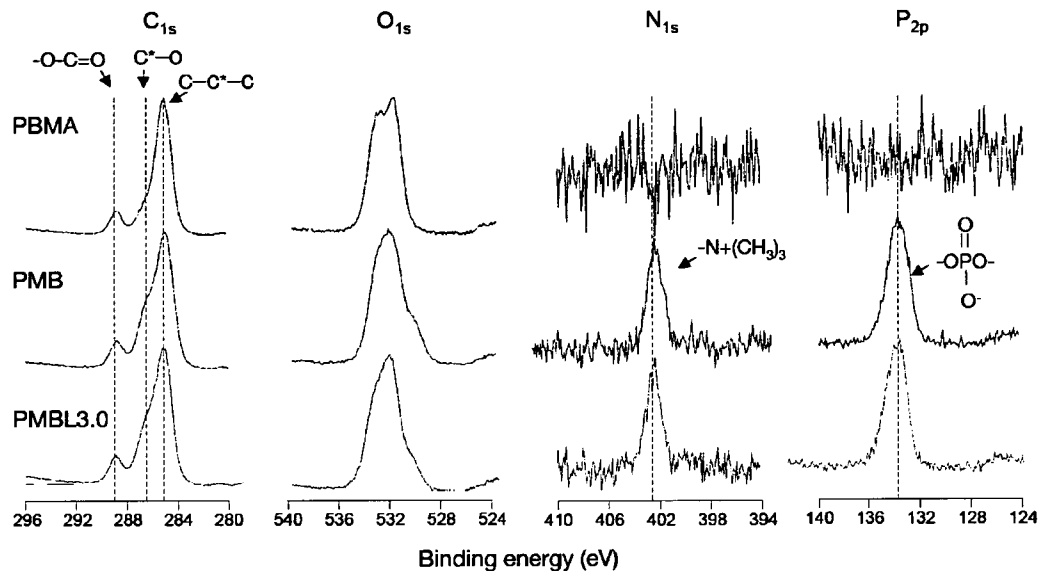


Figure 2. XPS spectra of polymer surfaces.

incubator with 95% humidity. After the cells were incubated on the polymer samples for the specific periods, the polymer plates were rinsed 3 times with PBS. The plates were then transferred to a new 24-well tissue culture plate. Triton X-100 (0.5 wt %, 1 mL) was introduced into each well, and the cells were incubated for 30 min. The Triton X-100 solution (250 μ L) was collected, and the concentration of LDH from the adherent cells was measured with an LDH-Cytotoxic Test kit (Wako Pure Chemical Industries, Ltd.).^{37,38}

Morphological observation of the HepG2 cells cultured on the polymer surfaces was performed using a confocal laser scanning microscope (LSM510, Zeiss). Cultured cells were fixed at 37 °C with 4% para-formaldehyde in Dulbecco's PBS for 20 min. The fixed surfaces were washed with PBS and permeabilized with 0.5% Triton X-100 in PBS for 2 min. The surfaces were then blocked with 0.1% BSA in PBS for 90 min. To enable observation of the cell membrane, a DMSO solution (10 μ L) of 10 μ M Texas Red-DHPE (Molecular Probes Inc.) and 0.1% BSA/PBS (1 mL) was poured into each well and stored for 30 min. After being rinsed with 0.1% BSA/PBS (1 mL) 3 times, F-actin synthesized in the cells was stained for assay by immunocytochemistry. The cells were in contact with primary antibodies [anti-human actin goat polyclonal antiserum (Sigma Chemical)], rinsed with PBS, and then incubated with FITC conjugated secondary antibody [FITC conjugated anti-goat IgG rabbit IgG (Sigma Chemical)]. The surfaces were then sufficiently rinsed with 0.1% BSA/PBS after which they were mounted for observation.

Albumin secreted from the HepG2 cells cultured on the polymer surfaces was determined by an enzyme linked immunosorbent assay (ELISA). After the HepG2 cells on the polymer surfaces were cultured for 96, 168, or 360 h, the culture medium was entirely changed, and additional culturing was continued for 24 h. The supernatant of the medium was collected, and the concentration of albumin was determined.

Statistical Analysis. The data are represented as the mean + the standard deviation (SD). Statistical comparisons ($n = 4$) were performed with the Student's t test.

Results and Discussion

Polymer Synthesis. To control biorecognition, polymer surfaces containing phospholipid polar groups and carbohydrates were designed as biomimetics of the outer surface of a biomembrane. Carbohydrate residues were added to the phosphorylcholine polymer surfaces as recognition sites. Figure 1 shows the structures of the polymers synthesized in this study. The polymerization of MPC, BMA, and LAMA was carried out in a DMSO mixture. As indicated in Table 1, the feed could be used to control the composition of each monomer unit. Copolymers containing various amounts of carbohydrate units were thus obtained. PET plates coated with the synthesized polymers from a 0.5 wt % solution were prepared by solvent evaporation. Elemental analysis of polymer-coated PET surfaces was performed by XPS. In the case of the PET plates coated with MPC polymers, nitrogen and phosphorus peaks were observed at 402.5 and 133.0 eV, respectively (Figure 2). O_{1s} shows a low binding energy component around 530 eV, which is most probably due to the PO_4 environment in phosphorylcholine. The XPS elemental concentration was summarized in Table 1. The concentration of oxygen was slightly increased by the addition of the LAMA unit to the copolymer. This increase is due to the hydroxyl groups of the carbohydrates and the LAMA units located on the surface of the sample plates.

Selective Binding of Lectin on Polymer Surfaces. To identify the selective interaction of lectin on the PMBL surface, the binding behavior was monitored by SPR. Figure 3 shows time courses of the change in the resonance angle of SPR responding to the addition of RCA₁₂₀ to a PMBL3.0-coated gold surface in PBS (pH 7.4). The change in the resonance angle ($\Delta\theta$) due to RCA₁₂₀ binding to PMBL3.0 was remarkable and well-correlated with the concentration of RCA₁₂₀. The apparent binding constant of RCA₁₂₀ to PMBL3.0 per LAMA unit was

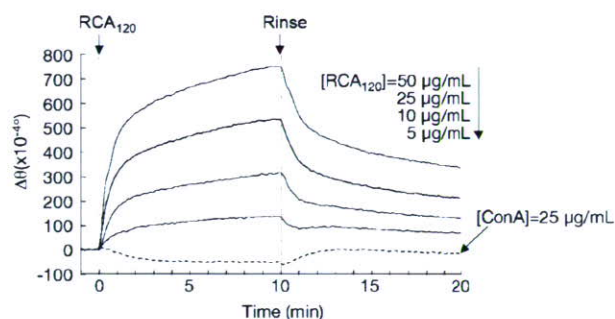


Figure 3. SPR curve on PMBL3.0 after contact with RCA120.

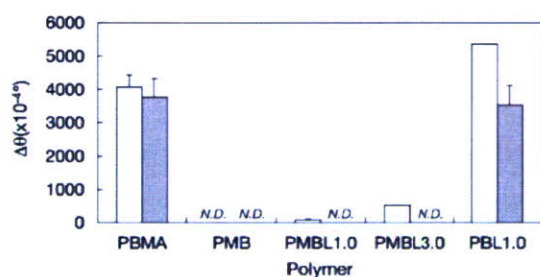


Figure 4. Change in the resonance angle of polymer-coated SPR sensors after contact with lectin for 10 min: (white) RCA₁₂₀ and (gray) Con A.

$2.77 \times 10^5 \text{ M}^{-1}$. Because these values are comparable to the affinity constant between the lactose-carrying polymer and RCA₁₂₀, it can be said that the conjugate is strongly bound to the lectin by the glycocluster effect.^{39,40} When Con A was in contact with the PMBL3.0-coated gold surface, the resonance angle was minimally changed, as shown in Figure 3. The $\Delta\theta$ value of various SPR sensor-coated polymers due to lectin binding is summarized in Figure 4. On PBMA and PBL1.0, $\Delta\theta$ was remarkable after contact both with RCA₁₂₀ and with Con A. This result indicates that nonspecific adsorption of lectin occurred on these surfaces. In contrast, $\Delta\theta$ was only detected on PMBL when RCA₁₂₀ was in contact with the surface; it increased with an increase in the fraction of the LAMA unit in PMBL. Although the absolute amount of RCA₁₂₀ adsorbed on the PMBL1.0 surface was much lower than that adsorbed on the PBL1.0 surface, nonspecific adsorption of Con A was completely reduced on the PMBL1.0 surface.

On the PMB surface, the resonance angle was minimally changed. The behavior of protein adsorption resistance on MPC polymer surfaces has been reported in past literature.²⁹ The phosphorylcholine group of MPC polymers is very hydrophilic, which means that hydrophobic interaction with proteins is unlikely. Moreover, phosphorylcholine polymers minimally interact with the water structure around the polymer.⁴¹ This is a unique property of phosphorylcholine polymers in comparison with the properties of conventional hydrophilic polymers. In addition, electrostatic interactions between a phosphorylcholine polymer surface and proteins are weak because the charge potential (ζ -potential) of phosphorylcholine is neutral.⁴² Therefore, a phosphorylcholine polymer has several features that reduce nonspecific protein adsorption. Consequently, this polymer is one of the best polymer materials for forming nonbiofouling surfaces.

The XPS concentrations of oxygen and phosphorus of PMBL-coated surfaces were higher than the theoretical amount calculated from the bulk concentration, as is shown in Table 1. Thus, both functions of MPC and LAMA units represent preferable surface properties. A few mole percent of LAMA

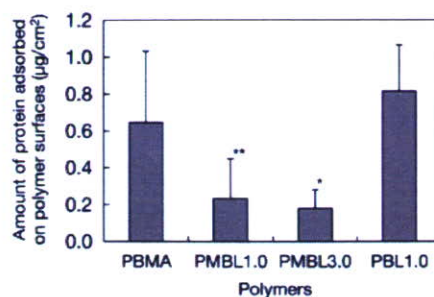


Figure 5. Amount of serum protein adsorbed on polymer surfaces after contact with cell culture medium for 60 min. * $p < 0.01$ PMBL3.0 vs PBMA and PMBL1.0 and ** $p < 0.05$ PMBL1.0 vs PBL1.0.

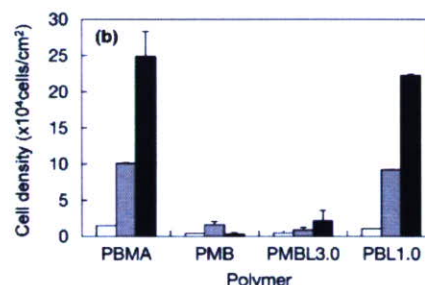
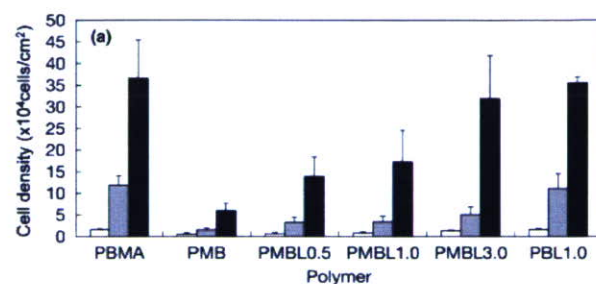


Figure 6. (a) Surface density on polymer surfaces after contact with HepG2 cells: (white) 24 h; (gray) 96 h; and (black) 168 h. (b) Surface density on polymer surfaces after contact with NIH/3T3 cells: (white) 24 h; (gray) 96 h; and (black) 168 h.

units incorporated into the copolymer did not influence the nonfouling properties of the MPC polymers and worked well as recognition sites for specific proteins.

Cell Culture Experiment. The amount of adsorbed protein on the polymer surfaces is shown in Figure 5. The PMBL1.0 and -3.0 surfaces significantly reduced protein adsorption as compared to that on PBL1.0. The amount of protein adsorption on PMBL is similar to that on PMB, as previously described.²⁹ The amount of protein adsorption on PMBL is a level for the reduction of nonspecific cell adhesion.²⁷

Figure 6a,b shows the time-dependent surface density of HepG2 and NIH-3T3 cells on a polymer surface after culturing for given periods, respectively. On a PBMA surface, many cells adhered, and the density increased with an increase in culture time. In contrast, cell adhesion was reduced on the PMB surface because adsorption of the cell adhesive protein on the surface could be reduced. Because the HepG2 cells have ASGPRs, which are galactose-recognizing receptors, cell adhesion was induced on the phosphorylcholine polymer surface having LAMA units. The cell density increased with an increase in the composition of LAMA units in the copolymers. When the LAMA composition was 3%, the density was similar to that on PBMA for every culture period (Figure 6a, PMBL3.0: * $p > 0.05$ vs PBMA and PBL1.0 and ** $p < 0.01$ vs PMB).

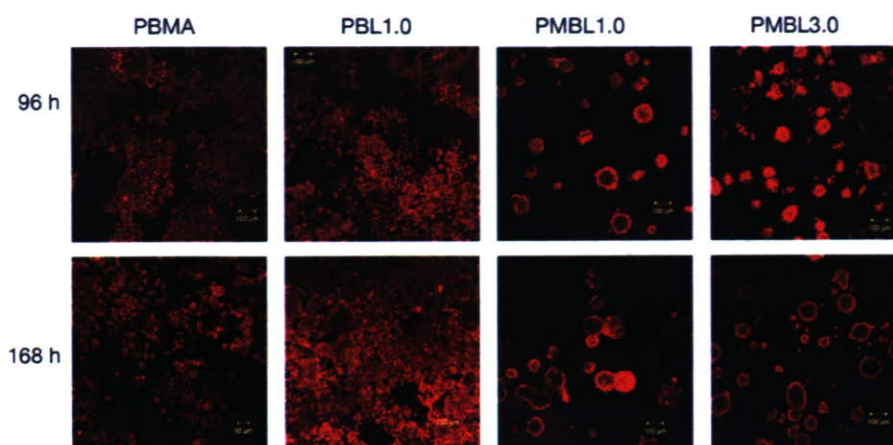


Figure 7. Fluorescence micrographs of polymer surfaces in contact with HepG2 cells for 96 and 168 h.

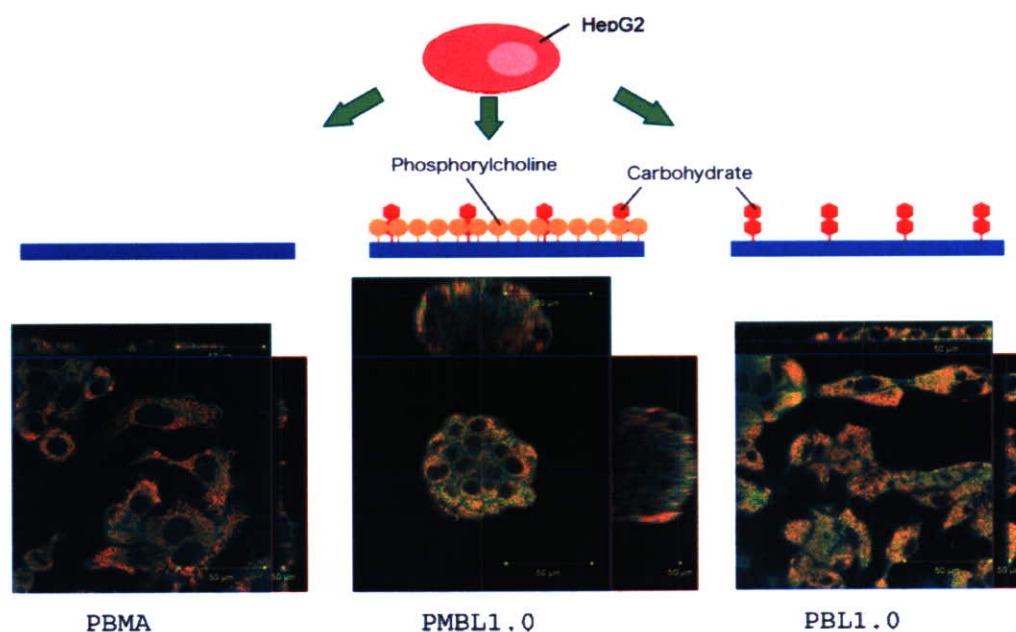


Figure 8. Confocal micrographs of adherent cells: (Green) F-actin and (red) phospholipid double layer.

NIH-3T3 cells do not have ASGPRs. On the PBMA surface, NIH-3T3 cells adhered and proliferated as well as the HepG2 cells did because much cell adhesive protein was adsorbed on the PBMA.²⁷ The LAMA unit in PBL did not affect NIH-3T3 cell adhesion, and a large number of NIH-3T3 cells adhered to the PBL1.0 surface. Because the PBL1.0 surface has a large amount of adsorbed protein containing cell adhesive protein such as fibronectin, integrin-mediated adhesion of NIH-3T3 cells on the PBL1.0 surface must have occurred. In contrast, the adhesion of NIH-3T3 cells was reduced on the polymer surfaces having MPC units (Figure 6b, PMBL3.0: $*p < 0.01$ vs PBMA and PBL1.0 and $**p > 0.05$ vs PMB). This result indicates that the ligand–receptor interaction at the polymer–cell interface worked preferably on the MPC polymers.

Spheroid Formation of HepG2 Cells. Figure 7 shows fluorescence micrographs of HepG2 cells cultured on polymer surfaces for 96 and 168 h. The membrane of the adherent cells was stained by Texas Red-DHPE. The adherent HepG2 cells on the PMBA surface were spread, and the morphology of each cell was easily observed. The HepG2 cells were also spread on the PBL1.0 surface, but some aggregation was observed. In contrast, the HepG2 cells observed on the PMBL1.0 and

PMBL3.0 surfaces formed spheroids. The number of spheroids on PMBL increased with an increase in the number of LAMA units in the copolymer. The average diameter of the spheroids under each condition was calculated by measuring 50 random samples. Each amount was found to be as follows: $86.1 \pm 26.7 \mu\text{m}$ (PMBL1.0, 96 h), $92.0 \pm 28.9 \mu\text{m}$ (PMBL3.0, 96 h), $115.7 \pm 28.6 \mu\text{m}$ (PMBL1.0, 168 h), and $125.8 \pm 29.1 \mu\text{m}$ (PMBL3.0, 168 h). The number of cells forming a spheroid was calculated from the data shown in Figures 6a and 7 and was around 25 cells for the 96 h culture and 125 cells (PMBL1.0) and 160 cells (PMBL3.0) for the 168 h culture. The size of the spheroids increased with an increase in the number of LAMA units, indicating that the units play a role in holding the spheroids to the polymer surface.

For spheroid formation, a round-bottomed plate with a nonbinding surface was generally used. Although the process was very successful, only one large spheroid per well was obtained, and nutrition did not reach inside the cells of a spheroid, resulting in necrosis. In addition to the process of using round-bottomed wells with a nonbinding surface, spheroid formation of hepatocytes has been studied on polymer surfaces controlled chemically and/or physically. Akaike and co-workers

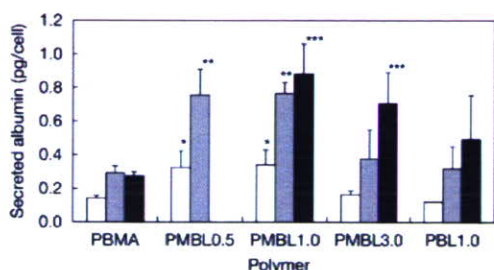


Figure 9. Amount of albumin secreted from adherent cells for 24 h after culturing of HepG2 cells on polymer surfaces for 96 (white), 168 (gray), and 360 h (black). * $p < 0.05$ vs PBMA in 96 h culture; ** $p < 0.01$ vs PBMA in 168 h culture; and *** $p < 0.01$ vs PBMA in 360 h culture.

are leading this field with the use of poly(*p*-*N*-vinylbenzyl-D-lactonamido) (PVLA). They reported that spheroid formation of hepatocytes on a PVLA surface could be observed with the addition of an epidermal growth factor (EGF).⁴³ The spheroid formation was also influenced by the morphologies of polymer surfaces such as honeycomb⁴⁴ and nanofibril⁴⁵ structures. On a PMBL surface, spheroid formation was induced on a flat surface and without the need for any growth factor or cytokine.

Figure 8 shows confocal micrographs of HepG2 cells cultured on PBMA, PBL1.0, and PMBL1.0 for 168 h. On PBMA and PBL1.0 surfaces, monolayer cell adhesion was observed, and each cell was spread. At the outline of the pseudo-pod formation of the adherent cells, actin was easily observed. In contrast, HepG2 cells cultured on PMBL1.0 formed spheroids with multilayer adhesion.

The mechanism of spheroid formation induced on PMBL surfaces is considered a nonintegrin-mediated adhesion phenomenon. The PMBL surfaces effectively reduce protein adsorption; the number of integrin binding sites on the surface is fewer than that on PBMA or PBL1.0 surfaces.

Albumin Secretion from Adherent HepG2. The functioning of HepG2 cells cultured on polymer surfaces was compared by measuring the amount of albumin secreted by the cells. Figure 9 shows the amount of albumin secreted by HepG2 cells for 24 h after 96 h (4 days), 168 h (7 days), and 360 h (15 days) of culturing on the polymer surfaces as determined by ELISA. At up to 168 h of culturing, the amount of albumin secreted per cell that adhered onto PMBL0.5 and -1.0 was significantly higher (* $p < 0.05$, 96 h and ** $p < 0.01$, 168 h) than that on PBMA and PBL1.0. After culturing for 360 h, high amounts of albumin secreted from cells that adhered onto PMBL1.0 and -3.0 were observed (** $p < 0.01$). On PMBL0.5, reproducible data for 360 h of culturing were not obtained because the spheroids were easily detached from the surface. The density of the LAMA unit on the PMBL1.0 surface appeared to be optimal for preserving the ability to secrete albumin. Lu et al. recently reported that the functional maintenance of hepatocytes was enhanced with NIH/3T3 fibroblasts.⁴⁶ Although the mechanism has not been explained in detail, cell contact with NIH/3T3 cells constitutes a better condition for hepatocytes. PMBL has phosphorylcholine groups similar to the cell surface, and the surface may present a more suitable situation for hepatocyte growth as compared to that of PBMA or PBL.

There has been great interest in the potential utility of a bioartificial liver (BAL) device as a bridge support for patients who have suffered massive liver injury during the period until the regeneration of their own hepatocytes or until liver transplantation. Although preservation of cell function in the material surface is very important for this application, conventional polymer materials such as polysulfone, polyolefine, and

polyurethane have generally been used.^{47,48} Surface modification is important in further improving the function of BAL devices. We have reported that MPC polymers could be applied in the surface modification of hollow fibers that have the possibility of producing hemodialyzer and liver assist bioreactor devices.^{49,50} We have applied PMBL as a coating material for polypropylene hollow fiber mini-modules, which are the subject of a long-term cell culture study. PMBL can reduce nonspecific biofouling, thus efficiently preserving the mass transport ability of hollow fiber membranes. In addition, the polymer can provide a more suitable environment for cell cultivation than that of conventional hollow fiber materials.

Conclusion

Carbohydrate-immobilized phosphorylcholine polymers (PMBL) were newly synthesized to produce biomembrane mimetic surfaces, which perform selective recognition of proteins and cells. Surfaces coated with PMBL effectively reduced nonspecific interactions, and a specific ligand-receptor interaction was clearly demonstrated. In this study, we used HepG2 cells to recognize galactose. The morphology of the cells and their functions on a PMBL surface were significantly different from those on a PBMA surface. LAMA units and MPC units of PMBL are important for supporting hepatocytes and for reducing nonspecific interactions at the cell-material interface, respectively. Yin et al. compared the morphology of cancer cells and primary cells on galactose-immobilized substrates.⁵¹ They stated that no significant difference in spheroid formation based on these cells was observed. Therefore, the primary hepatic cell might form spheroids on the PMBL surface. The primary cell function on the PMBL surface will be reported in the near future.

We clarified that carbohydrates immobilized on the phosphorylcholine polymer surface were easily distinguished from the specific protein and cells. Changing the types of carbohydrates enables changes in the types of biorecognition. The polymers have great potential for bioreaction, molecular separation, targeting, sensing, etc.

Acknowledgment. We thank the New Energy and Industrial Technology Development Organization (NEDO) Japan (Industrial Technology Research Grant in 2004, 04A02025) for providing financial support.

References and Notes

- (1) Ratner, B. D. The engineering of biomaterials exhibiting recognition and specificity. *J. Mol. Recognit.* **1996**, *9*, 617–625.
- (2) Ratner, B. D. New ideas in biomaterials science—A path to engineered biomaterials. *J. Biomed. Mater. Res.* **1993**, *27*, 837–850.
- (3) Lee, J. H.; Lee, H. B. A wettability gradient as a tool to study protein adsorption and cell adhesion on polymer surfaces. *J. Biomater. Sci., Polym. Ed.* **1993**, *4*, 467–481.
- (4) Mrksich, M.; Chen, C. S.; Xia, Y.; Dike, L. E.; Ingber, D. E.; Whitesides, G. M. Controlling cell attachment on contoured surfaces with self-assembled monolayers of alkanethiols on gold. *Proc. Natl. Acad. Sci. U.S.A.* **1996**, *93*, 10775–10778.
- (5) Ito, Y. Surface micropatterning to regulate cell functions. *Biomaterials* **1999**, *20*, 2333–2342.
- (6) Massia, S. P.; Hubbell, J. A. Human endothelial cell interactions with surface-coupled adhesion peptides on a nonadhesive glass substrate and two polymeric biomaterials. *J. Biomed. Mater. Res.* **1991**, *25*, 223–242.
- (7) Lin, H. B.; Garcia-Echeverria, C.; Asakura, S.; Sun, W.; Mosher, D. F.; Cooper, S. L. Endothelial cell adhesion on polyurethanes containing covalently attached RGD peptides. *Biomaterials* **1992**, *13*, 905–914.
- (8) Sugawara, T.; Matsuda, T. Photochemical surface derivatization of a peptide containing Arg-Gly-Asp (RGD). *J. Biomed. Mater. Res.* **1995**, *29*, 1047–1052.

- (9) Shakesheff, K.; Cannizzaro, S.; Langer, R. Creating biomimetic microenvironments with synthetic polymer-peptide hybrid molecules. *J. Biomater. Sci., Polym. Ed.* **1998**, *9*, 507–518.
- (10) VandeVondele, S.; Voros, J.; Hubbell, J. A. RGD-grafted poly-L-lysine-graft-(poly(ethylene glycol)) copolymers block non-specific protein adsorption while promoting cell adhesion. *Biotechnol. Bioeng.* **2003**, *82*, 784–790.
- (11) Murphy, W. L.; Mercurius, K. O.; Koide, S.; Mrksich, M. Substrates for cell adhesion prepared via active site-directed immobilization of a protein domain. *Langmuir* **2004**, *20*, 1026–1030.
- (12) Hersel, U.; Dahmen, C.; Kessler, H. RGD modified polymers: Biomaterials for stimulated cell adhesion and beyond. *Biomaterials* **2003**, *24*, 4385–4415.
- (13) Massia, S. P.; Hubbell, J. A. An RGD spacing of 440 nm is sufficient for integrin $\alpha V \beta 3$ -mediated fibroblast spreading and 140 nm for focal contact and stress fiber formation. *J. Cell Biol.* **1991**, *114*, 1089–1100.
- (14) Kobayashi, A.; Kobayashi, K.; Akaike, T. Control of adhesion and detachment of parenchymal liver cells using lactose-carrying polystyrene as substratum. *J. Biomater. Sci., Polym. Ed.* **1992**, *3*, 499–508.
- (15) Gestwicki, J. E.; Cairo, C. W.; Mann, D. A.; Owen, R. M.; Kiessling, L. L. Selective immobilization of multivalent ligands for surface plasmon resonance and fluorescence microscopy. *Anal. Biochem.* **2002**, *305*, 149–155.
- (16) Pricer, W. E.; Hudgin, R. L.; Ashwell, G.; Stockert, R. J.; Morell, A. G. A membrane receptor protein for asialoglycoproteins. *Methods Enzymol.* **1974**, *34*, 688–691.
- (17) Stockert, R. J. The asialoglycoprotein receptor: Relationships between structure, function, and expression. *Physiol. Rev.* **1995**, *75*, 591–609.
- (18) Weigel, P. H.; Sennaar, R. L.; Kuhlenschmidt, M. S.; Schmell, E.; Lee, R. T.; Lee, Y. C.; Roseman, S. Adhesion of hepatocytes to immobilized sugars. A threshold phenomenon. *J. Biol. Chem.* **1979**, *254*, 10830–10838.
- (19) Kobayashi, A.; Akaike, T.; Kobayashi, K.; Sumitomo, H. Enhanced adhesion and survival efficacy of liver cells in culture dishes coated with a lactose-carrying styrene homopolymer. *Makromol. Chem., Rapid Commun.* **1986**, *7*, 645–650.
- (20) Gutsche, A. T.; Parsons-Wingeter, P.; Chand, D.; Saltzman, W. M.; Leong, K. W. *N*-Acetylglucosamine and adenosine derivatized surfaces for cell culture, 3T3 fibroblast, and chicken hepatocyte response. *Biotechnol. Bioeng.* **1994**, *43*, 801–809.
- (21) Sagara, K.; Kim, S. W. A new synthesis of galactose-poly(ethylene glycol)-polyethylenimine for gene delivery to hepatocytes. *J. Controlled Release* **2002**, *79*, 271–281.
- (22) Kim, S. H.; Hoshiba, T.; Akaike, T. Hepatocyte behavior on synthetic glycopolymer matrix: Inhibitory effect of receptor–ligand binding on hepatocyte spreading. *Biomaterials* **2004**, *25*, 1813–1823.
- (23) Sato, K.; Miura, Y.; Saito, N.; Kobayashi, K.; Takai, O. *Biomacromolecules* **2007**, *8*, 753–756.
- (24) Yarema, K. J.; Mahal, L. K.; Bruehl, R. E.; Rodriguez, E. C.; Bertozzi, C. R. Metabolic delivery of ketone groups to sialic acid residues. Application to cell surface glycoform engineering. *J. Biol. Chem.* **1998**, *273*, 31168–31179.
- (25) Iwasaki, Y.; Mikami, A.; Kurita, K.; Yui, N.; Ishihara, K.; Nakabayashi, N. Reduction of surface-induced platelet activation on phospholipid polymers. *J. Biomed. Mater. Res.* **1997**, *36*, 508–515.
- (26) Iwasaki, Y.; Sawada, S.; Nakabayashi, N.; Khang, G.; Lee, H. B.; Ishihara, K. The effect of the chemical structure of the phospholipid polymer on fibronectin adsorption and fibroblast adhesion on the gradient phospholipid surface. *Biomaterials* **1999**, *20*, 2185–2191.
- (27) Ishihara, K.; Ishikawa, E.; Iwasaki, Y.; Nakabayashi, N. Inhibition of fibroblast cell adhesion on substrate by coating with 2-methacryloyloxyethyl phosphorylcholine polymers. *J. Biomater. Sci., Polym. Ed.* **1999**, *10*, 1047–1061.
- (28) Iwasaki, Y.; Nakabayashi, N.; Ishihara, K. Preservation of platelet function on 2-methacryloyloxyethyl phosphorylcholine-graft polymer as compared to various water-soluble graft polymers. *J. Biomed. Mater. Res.* **2001**, *57*, 72–78.
- (29) Ishihara, K.; Oshida, H.; Endo, Y.; Ueda, T.; Watanabe, A.; Nakabayashi, N. Hemocompatibility of human whole blood on polymers with a phospholipid polar group and its mechanism. *J. Biomed. Mater. Res.* **1992**, *26*, 1543–1552.
- (30) Ishihara, K.; Nomura, H.; Mihara, T.; Kurita, K.; Iwasaki, Y.; Nakabayashi, N. Why do phospholipid polymers reduce protein adsorption? *J. Biomed. Mater. Res.* **1998**, *39*, 323–330.
- (31) Iwasaki, Y.; Sawada, S.; Ishihara, K.; Khang, G.; Lee, H. B. Reduction of surface-induced inflammatory reaction on PLGA/MPC polymer blend. *Biomaterials* **2002**, *23*, 3897–3903.
- (32) Sawada, S.; Sakaki, S.; Iwasaki, Y.; Nakabayashi, N.; Ishihara, K. Suppression of the inflammatory response from adherent cells on phospholipid polymers. *J. Biomed. Mater. Res.* **2003**, *64*, 411–416.
- (33) Ishihara, K.; Ueda, T.; Nakabayashi, N. Preparation of phospholipid polymers and their properties as polymer hydrogel membranes. *Polym. J.* **1990**, *22*, 355–360.
- (34) Narain, R.; Armes, S. P. Synthesis and aqueous solution properties of novel sugar methacrylate-based homopolymers and block copolymers. *Biomacromolecules* **2003**, *4*, 1746–1758.
- (35) Matsuura, K.; Kobayashi, K. Analysis of GM3–Gg3 interaction using clustered glycoconjugate models constructed from glycolipid monolayers and artificial glycoconjugate polymers. *Glycoconjugate J.* **2004**, *21*, 139–148.
- (36) Iwasaki, Y.; Fujiike, A.; Kurita, K.; Ishihara, K.; Nakabayashi, N. Protein adsorption and platelet adhesion on polymer surfaces having a phospholipid polar group connected with oxyethylene chain. *J. Biomater. Sci., Polym. Ed.* **1996**, *8*, 91–102.
- (37) Tsai, W. B.; Grunkemeier, J. M.; Horbett, T. A. Human plasma fibrinogen adsorption and platelet adhesion to polystyrene. *J. Biomed. Mater. Res.* **1999**, *44*, 130–139.
- (38) Haslam, G.; Wyatt, D.; Kitos, P. A. Estimating the number of viable animal cells in multi-well cultures based on their lactate dehydrogenase activities. *Cytotechnology* **2000**, *32*, 63–75.
- (39) Lee, Y. C. Biochemistry of carbohydrate–protein interaction. *FASEB J.* **1992**, *26*, 3193–3200.
- (40) Matsuura, K.; Hayashi, K.; Kobayashi, K. On-off switching of gene expression regulated with carbohydrate-lectin interaction. *Biomacromolecules* **2005**, *6*, 2533–2540.
- (41) Ishihara, K.; Nomura, H.; Mihara, T.; Kurita, K.; Iwasaki, Y.; Nakabayashi, N. Why do phospholipid polymers reduce protein adsorption? *J. Biomed. Mater. Res.* **1998**, *39*, 323–330.
- (42) Ishihara, K.; Inoue, H.; Kurita, K.; Nakabayashi, N. Selective adhesion of platelets on a polyion complex composed of phospholipid polymers containing sulfonate groups and quaternary ammonium groups. *J. Biomed. Mater. Res.* **1994**, *28*, 1347–1355.
- (43) Tobe, S.; Takei, Y.; Kobayashi, K.; Akaike, T. Receptor-mediated formation of multilayer aggregates of primary cultured adult rat hepatocytes on lactose-substituted polystyrene. *Biochem. Biophys. Res. Commun.* **1992**, *184*, 225–230.
- (44) Tanaka, M.; Nishikawa, K.; Okubo, H.; Kamachi, H.; Kawai, T.; Matsushita, M.; Todo, S.; Shimomura, M. Control of hepatocyte adhesion and function on self-organized honeycomb-patterned polymer film. *Colloids Surf., A* **2006**, *284*, 464–469.
- (45) Chua, K. N.; Lim, W. S.; Zhang, P.; Lu, H.; Wen, J.; Ramakrishna, S.; Leong, K. W.; Mao, H. Q. Stable immobilization of rat hepatocyte spheroids on galactosylated nanofiber scaffold. *Biomaterials* **2005**, *26*, 2537–2547.
- (46) Lu, H. F.; Chua, K. N.; Zhang, P. C.; Lim, W. S.; Ramakrishna, S.; Leong, K. W.; Mao, H. Q. Three-dimensional co-culture of rat hepatocyte spheroids and NIH/3T3 fibroblasts enhances hepatocyte functional maintenance. *Acta Biomater.* **2005**, *1*, 399–410.
- (47) Mizumoto, H.; Funatsu, K. Liver regeneration using a hybrid artificial liver support system. *Artif. Organs* **2004**, *28*, 53–57.
- (48) Long, L.; Liu, Z.; Wang, T.; Deng, X.; Yang, K.; Li, L.; Zhao, C. Polyethersulfone dead-end tube as a scaffold for artificial lacrimal glands in vitro. *J. Biomed. Mater. Res., Part B* **2006**, *78*, 409–416.
- (49) Hasegawa, T.; Iwasaki, Y.; Ishihara, K. Preparation of blood-compatible hollow fibers from a polymer alloy composed of polysulfone and 2-methacryloyloxyethyl phosphorylcholine polymer. *J. Biomed. Mater. Res.* **2002**, *63*, 333–341.
- (50) Ye, S. H.; Watanabe, J.; Takai, M.; Iwasaki, Y.; Ishihara, K. Design of functional hollow fiber membranes modified with phospholipid polymers for application in total hemopurification systems. *Biomaterials* **2005**, *26*, 5032–5041.
- (51) Yin, C.; Liao, K.; Mao, H. Q.; Leong, K. W.; Zhuo, R. X.; Chan, V. Adhesion contact dynamics of HepG2 cells on galactose-immobilized substrates. *Biomaterials* **2003**, *24*, 837–850.

Control of cell function on carbohydrate-immobilized phosphorylcholine polymer surfaces

Y.Iwasaki¹, U.Takami², Y.Shinohara², K.Akiyoshi²

¹ Kansai University, Osaka, Japan. ² Tokyo Medical and Dental University, Tokyo, Japan.

INTRODUCTION: We hypothesized that 2-methacryloyloxyethyl phosphorylcholine (MPC) polymer surfaces bearing carbohydrates might perform as biomembrane mimetic surfaces, which can interact with a specific cell. In this study, MPC copolymers with galactose residues have been synthesized and we present here the effectiveness of the surface in controlling cell/material interaction and preserving cell function.

METHODS: Poly[MPC-co-n-butyl methacrylate (BMA)] (PMB), poly[BMA-co-2-lactobionamidoethyl methacrylate (LAMA)] (PBL), and poly(MPC-co-BMA-co-LAMA) (PMBL) were synthesized by conventional radical polymerization¹.

Human hepatocellular liver carcinoma cell line (HepG2) cells and mouse fibroblasts (NIH-3T3) were purchased from RIKEN Cell Bank. The concentration of the cells was adjusted to 2.0×10^4 cells/ml. The cells were seeded on the polymer surfaces and continuously cultured for specific periods. The polymer plates were then rinsed with PBS. The plates were soaked into Triton X-100 aqueous solution. The Triton X-100 solution was collected and the concentration of LDH from the adherent cells was measured.

Morphological observation of the HepG2 cells cultured on the polymer surfaces was performed by a confocal laser scanning microscope.

RESULTS: Figure 1 shows the time-dependent surface density of HepG2 and NIH-3T3 cells on a polymer surface after culture for given periods. On a PBMA surface, many HepG2 cells adhered and the density increased with an increase in culture time. In contrast, the cell adhesion was reduced on the PMB surface because adsorption of

the cell-adhesive protein on the surface could be reduced (data not shown). When the LAMA composition was 3% in PMBL, the density of adherent HepG2 cells was similar to that on PBMA for every culture period. NIH-3T3 cells adhered and proliferated as well as the HepG2 cells on the PBMA surface. On the other hand, the adhesion of NIH-3T3 cells was reduced on the polymer surfaces having MPC units.

Figure 2 shows confocal micrographs of HepG2 cells cultured on PBMA, PBL1.0, and PMBL1.0 for 168 h. On PBMA and PBL1.0 surfaces, monolayer cell adhesion was observed and each cell was spread. At the outline of the pseudopod formation of the adherent cells, actin was easily observed. In contrast, HepG2 cells cultured on PMBL1.0 formed spheroids with multilayer adhesion.

DISCUSSION & CONCLUSIONS: Carbohydrate-immobilized phosphorylcholine polymers (PMBL) were newly synthesized to produce biomembrane mimetic surfaces, which perform selective recognition of proteins and cells. Surfaces coated with PMBL effectively reduced nonspecific interaction, and specific ligand/receptor interaction was clearly demonstrated. Changing the types of carbohydrates enables changes in the types of biorecognition. The polymers have great potential for bioreaction, molecular separation, targeting, sensing, etc.

REFERENCES: ¹ Y. Iwasaki, U.Takami, Y.Shinohara, et al (2007) *Biomacromolecules*, in press.

ACKNOWLEDGEMENTS: We thank the New Energy and Industrial Technology Development Organization (NEDO) Japan for providing financial support.

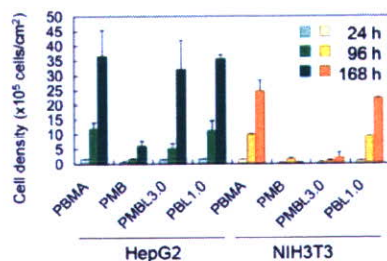


Fig. 1: Cell density on polymer surfaces.

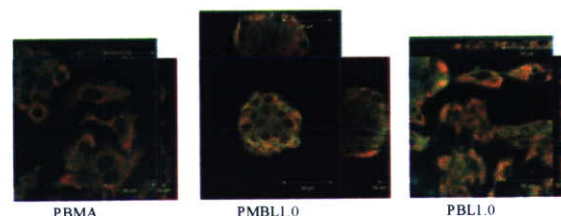


Fig. 2: Fluorescence micrographs of adherent cells.

Site-directed immobilization of antibodies on well-defined polymer brushesR.Iwata¹, Y.Iwasaki², K.Akiyoshi¹¹ *Institute of Biomaterials and Bioengineering, Tokyo Medical and Dental University, Tokyo, Japan.*² *Faculty of Chemistry, Materials and Bioengineering, Kansai University, Osaka, Japan.*

INTRODUCTION: Surface characteristics for biosensor applications require both reducing non-specific biofouling and enhancing specific recognition. Especially in the protein-chip technology, immobilization of proteins in proper orientation is necessary to maintain the biological activities. We have reported that 2-methacryloyloxyethyl phosphorylcholine (MPC) polymers synthesized as biomimetics in biomembrane structures significantly reduce protein adsorption and cell adhesion¹. Furthermore, manipulation of protein and cell was well performed on well-defined poly(MPC) (PMPC) brushes produced by atom transfer radical polymerization (ATRP)². The block copolymer brushes consisting of PMPC and poly[glycidyl methacrylate (GMA)] were also recently prepared for engineered biomaterial surfaces³. We describe here about oriented immobilization of antibodies onto the polymer brushes for biorecognition surfaces.

METHODS: Polymer brushes consisting of PMPC and poly(GMA) (PGMA) were formed on silicon wafers by ATRP as described previously³. Pyridyl disulfide moieties were then introduced to the polymer brushes via epoxy groups in GMA unit. Fab' fragments (Goat anti-mouse IgG) solution was in contact with polymer brushes with pyridyl disulfide moieties and reacted at room temperature over night. After the immobilization of Fab' fragments and wash with buffer, 1% bovine serum albumin (BSA) was applied to surfaces and incubated for 1h at room temperature. Fluorescein isothiocyanate- (FITC-) labeled immunoglobulin (Mouse anti-rat IgG) was used as antigen. BSA solution was removed and antigen solution was in contact with polymer brushes with Fab' fragments for 1 h at room temperature. After wash and dried, the fluorescence intensity was analyzed.

RESULTS: Fab' fragment is one of the antibody fragments and has thiol group in the opposite side of antigen-binding domain. We can immobilize the Fab' fragments in ordered orientation via thiol-disulfide exchange between the thiol groups of Fab' fragments and pyridyl disulfide moieties in polymer brushes. To compare the amount of immobilized antibody, FITC-labeled Fab'

fragments were reacted with each surfaces and the fluorescence intensity was determined. We prepared the organosilane monolayer having epoxy groups (epoxysilane films) as a control surface. The amount of immobilized antibody increased with an increase in the length of GMA unit. PGMA brush immobilized largest amount of antibody. Fig. 1 shows the ratio of fluorescence intensity of each surface after contact with FITC-labeled antigen. The fluorescence intensity of polymer brushes was higher than that of epoxysilane. In PMPC-*b*-PGMA brushes, the fluorescence intensity increased with an increase in the thickness of PGMA.

DISCUSSION & CONCLUSIONS: The amount of immobilized Fab' fragments and subsequent reaction with antigen could be controlled by changing the thickness of polymer brushes. Although PGMA brush surface has larger amount of Fab' fragment compared with PMPC-*b*-PGMA brush with longer PGMA, the reactivity with antigen was similar on these surfaces (Fig. 1.). It is considered that the condition of immobilized Fab' fragments are different between PGMA brush and PMPC-*b*-PGMA brush which has biocompatible PMPC under PGMA. It was also shown that polymer brush surface for reaction with antigen was more effective than the epoxysilane films. The characteristics of PMPC and dense immobilization of antibodies in defined orientation are effective in high sensitive biorecognition.

REFERENCES: ¹S. Sawada, S. Sakaki, Y. Iwasaki, N. Nakabayashi, K. Ishihara (2003) *J Biomed Mater Res* **64A**:411-416. ²R. Iwata, P. Suk-In, V.P. Hoven, A. Takahara, K. Akiyoshi, Y. Iwasaki (2004) *Biomacromolecules* **5**:2308-2314. ³R. Iwata, Y. Iwasaki, K. Akiyoshi, A. Takahara (2005) *Trans. Mater. Res. Soc. Jpn* **30**:735-738.

ACKNOWLEDGEMENTS: The authors of this paper would like to thank Japan Society for the Promotion of Science for financial support of this research.

Novel Thermoresponsive Polymers Having Biodegradable Phosphoester Backbones

Yasuhiko Iwasaki,*[†]
Chookaet Wachiralarpphaithoon,[‡] and
Kazunari Akiyoshi[§]

Department of Chemistry and Materials Engineering,
Faculty of Chemistry, Materials and Bioengineering, Kansai
University, 3-3-35 Yamate-cho, Suita-shi, Osaka 564-8680,
Japan. Institute of Biomaterials and Bioengineering, Tokyo
Medical and Dental University, 2-3-10 Kanda-surugadai,
Chiyoda-ku, Tokyo 101-0062, Japan, and Center of
Excellence Program for Frontier Research on Molecular
Destruction and Reconstruction of Tooth and Bone, Tokyo
Medical and Dental University, 2-3-10 Kanda-surugadai,
Chiyoda-ku, Tokyo 101-0062, Japan

Received July 13, 2007

Revised Manuscript Received September 24, 2007

Introduction. Thermoresponsive polymers are widely studied in both research and technology because of their versatility in many fields. Recent trends in polymer materials are drug delivery,¹ separation of bioactive molecules,² and tissue engineering.³ *N*-substituted acrylamide polymers have been found to have a phase separation characteristic with changes occurring in their properties upon heating above a certain lower critical solution temperature (LCST).^{4–6} In particular *N*-isopropylacrylamide (NIPAAm) is one of the best monomers for accomplishing this and the homopolymer has LCST at 32 °C in aqueous solution.⁷ NIPAAm can be applied to polymerization with a wide variety of comonomers and the LCST of the polymers can be controlled around physiological temperatures.^{8,9} Furthermore, living radical polymerization has recently been applied with NIPAAm for the preparation of smart polymers with well-defined structures.^{10–12} Although NIPAAm is a robust monomer for obtaining thermoresponsive polymer materials such as stimuli-responsive surfaces, particles, and hydrogels, the polymers are not biodegradable.

As well as a stimuli-responsive nature, biodegradability and biocompatibility are important characteristics for polymeric materials used in biomedical fields. While the thermoresponsivity of some biodegradable polymers such as aliphatic polyester block copolymers or polypeptides was recently proposed,^{13–16} the molecular design and synthetic process of thermoresponsive biodegradable polymers are still limited. *N*-substituted acrylamide polymers are thus preferably studied.

Recently, polyphosphoesters have appeared interesting for biological and pharmaceutical applications because of their biocompatibility and structural similarities to naturally occurring nucleic and teichoic acids. Polyphosphoesters have been proposed for use in the field of biomaterials.^{17–20} A variety of synthetic routes for polyphosphoesters has been proposed including ring-opening polymerization,^{21,22} polycondensation,²³ transesterification,^{24,25} and enzymatic polymerization.²⁶ There has

been a great deal of interest in polyphosphoesters, which are biodegradable through hydrolysis and possibly through enzymatic digestion of phosphate linkages under physiological conditions.²⁷ Although polyphosphoesters are very interesting polymers, there is no report of any thermoresponsive properties. In current research, thermoresponsive polyphosphoesters are being newly synthesized with simple copolymerization of cyclic phosphoester compounds and their properties are being investigated.

Results and Discussion. 2-Ethoxy-2-oxo-1,3,2-dioxaphospholane (EP) and 2-isopropoxy-2-oxo-1,3,2-dioxaphospholane (IPP) were synthesized by the previously described method.²⁸ Poly(IPP-co-EP) (PI_xE_yP; *x* = IPP (mol %); *y* = EP (mol %)) was synthesized by ring-opening polymerization using triisobutyl aluminum (*i*Bu₃Al) as an initiator (Scheme 1). The polymerization was homogeneously performed by a solvent-free reaction. The polymers were dissolved in ethanol and purified by reprecipitation into diethyl ether. The range of weight-averaged molecular weights was 1.2 × 10⁴ to 1.5 × 10⁴ g/mol by gel-permeation chromatography through a Polymer Laboratories MIXED-C column using a calibration curve based on linear polystyrene standards and their molecular weight distribution was lower than 1.3. Chloroform was the GPC solvent. The molar fraction of IPP and EP in the copolymer was calculated from a ¹H NMR spectrum. ¹H NMR (270 MHz, CDCl₃): δ = PI_xE_yP: 1.21–1.47 (m; –CH₃, 6H in IPP and 3H in EP), 3.95–4.20 (m; –CH₂–, 2H in EP and –OCH₂CH₂O–, 4H in backbone), 4.58 (m; –CH(CH₃)₂ in IPP, 1H).

The polymerization ratio (*r*₁/*r*₂) of IPP and EP was 0.48/2.23 as determined by the Fineman-Ross method. The reactivity of EP was much higher than that of IPP. Chen and co-workers compared the polymerization ability of IPP and EP using stannous octoate as an initiator.²⁹ In their data, the higher reactivity of EP was also observed.

Figure 1 is a typical photograph of aqueous solutions of PI₂₄E₇₆P, which has 24-mol % IPP and 76-mol % EP. The solution was transparent at 20 °C, but it was turbid at 40 °C. The LCST of PI₂₄E₇₆P was 31 °C, as determined from the middle point of the transition state of transmittance using JASCO software.

Figure 2 shows the effect of the composition of the monomer unit on the LCST of the copolymers. The LCST of poly(EP) (PEP) was 38 °C and it linearly decreased with an increase in the composition of IPP. IPP is relatively hydrophobic, the homopolymer of IPP is not soluble in water above 5 °C. Dehydration of the polymer then preferably occurred with the addition of the hydrophobic IPP unit. It is reported that the LCST of thermoresponsive polymers can be controlled by compositions of hydrophobic and hydrophilic units.^{8,15} Thermoresponsivity under physiological conditions is effective for drug delivery or tissue engineering applications.^{30,31} The thermoresponsivity of polyphosphoesters can also be observed under physiological temperatures. Thus, the polymers are applicable in biomedical field.

Figure 3 shows the repeated temperature dependence of the transmittance of light through a PI₂₄E₇₆P aqueous solution. While the hysteresis of change in transmittance between the variations in temperature was observed, the curve coincided well with the variation regardless of the number of repetitions. The polymer associate then completely disintegrated at the low temperature. The hydrodynamic radii (*R*_h) of PI₂₄E₇₆P in an

* Corresponding author. Fax: +81-6-6368-0090. Telephone: +81-6-6368-0090. E-mail: yasu.bmt@ipc.ku.kansai-u.ac.jp.

[†] Department of Chemistry and Materials Engineering, Faculty of Chemistry, Materials and Bioengineering, Kansai University.

[‡] Institute of Biomaterials and Bioengineering, Tokyo Medical and Dental University.

[§] Center of Excellence Program for Frontier Research on Molecular Destruction and Reconstruction of Tooth and Bone, Tokyo Medical and Dental University.

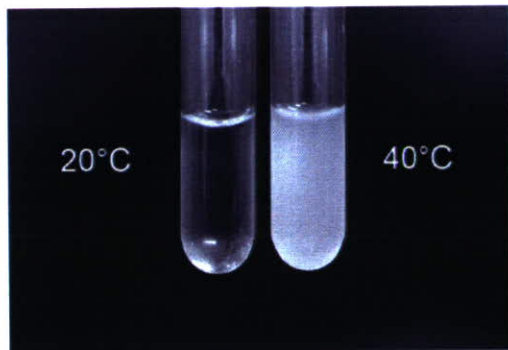
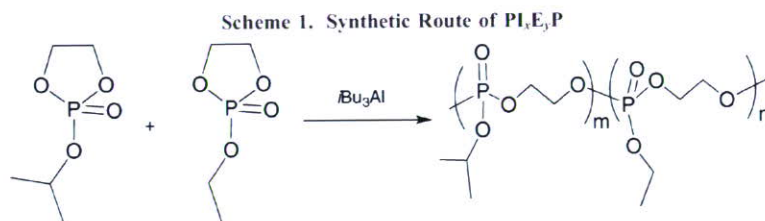


Figure 1. Photograph of PI₂₄E₇₆P aqueous solution at 20 and 40 °C.

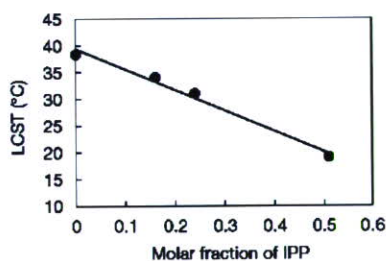


Figure 2. Effect of molar fraction of IPP on LCST of PI₂₄E₇₆P.

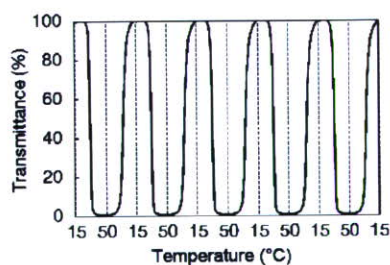


Figure 3. Change in the transmittance of polymer solution by repeated thermal cycling.

aqueous solution were also investigated using the Malvern dynamic light scattering technique. When the R_h of PI₂₄E₇₆P at below 20 °C was 6.7 ± 0.1 nm, the polymer associate with more than $6 \mu\text{m}$ R_h was formed at 50 °C. The phase separation behavior of the polymer was easily reproducible.

Hydrogels^{30,31} and nanoparticles^{32,33} have been prepared using polyphosphoesters as macrocross-linkers and macroinitiators, respectively. In the former literatures, the enzymatic digestion and nonenzymatic degradation of polyphosphoesters were investigated. Typically, the rate of degradation of a hydrogel cross-linked with polyphosphoesters was increased with an increase in the concentration of alkaline phosphatase in the soaking medium. Furthermore, the cytotoxicity of the polyphosphoesters and the degradation products were not observed. These polyphosphoesters have been recently studied as artificial cellular matrices and nanoparticles for drug delivery systems.

The possibility of varied molecular designs and changeable solubility of polyphosphoesters can be looked upon as an

advantage of the polymers in comparison with conventional biodegradable polymers such as aliphatic polyesters.

In conclusion, thermoresponsive polyphosphoesters were newly obtained from the copolymerization of two cyclic phosphoester monomer components. The LCST of the copolymers could be easily controlled with the composition and the thermoresponsivity of the polymers was ably reproducible. Thermoresponsive polyphosphoesters have great potential as novel smart biomaterials.

Acknowledgment. The authors acknowledge financial support from Mukai Science and Technology Foundation. The authors are grateful to Mr. Kazuaki Ikoma and Mr. Takashi Kawakita for their experimental support.

Supporting Information Available: Text giving experimental procedures and synthetic results of polymers, a table of synthetic results, and a figure showing the effect of temperature on light transmittance. This material is available free of charge via the Internet at <http://pubs.acs.org>.

References and Notes

- Kikuchi, A.; Okano, T. *Adv. Drug Deliv. Rev.* **2002**, *54*, 53–77.
- Kobayashi, J.; Kikuchi, A.; Sakai, K.; Okano, T. *Anal. Chem.* **2003**, *75*, 3244–3249.
- Kikuchi, A.; Okano, T. *J. Controlled Release* **2005**, *101*, 69–84.
- Monji, N.; Cole, C. A.; Hoffman, A. S. *J. Biomater. Sci., Polym. Ed.* **1994**, *5*, 407–420.
- Yamazaki, A.; Winnik, F. M.; Cornelius, R. M.; Brash, J. L. *Biochim. Biophys. Acta* **1999**, *1421*, 103–115.
- Idziak, I.; Avoce, D.; Lessard, D.; Gravel, D.; Zhu, X. X. *Macromolecules* **1999**, *32*, 1260–1263.
- Heskins, M.; Guillent, J. E.; James, E. J. *Macromol. Sci. Chem.* **1968**, *A2*, 1441–1445.
- Takei, Y. G.; Aoki, T.; Sanui, K.; Ogata, N.; Okano, T.; Sakurai, Y. *Bioconjug. Chem.* **1993**, *4*, 341–346.
- Feil, H.; Bae, Y. H.; Feijen, J.; Kim, S. W. *Macromolecules* **1993**, *26*, 2496–2500.
- Hales, M.; Barner-Kowollik, C.; Davis, T. P.; Stenzel, M. H. *Langmuir* **2004**, *20*, 10809–10817.
- Kulkarni, S.; Schilli, C.; Grin, B.; Muller, A. H. E.; Hoffman, A. S.; Stayton, P. S. *Biomacromolecules* **2006**, *7*, 2736–2741.
- Lokuge, I.; Wang, X.; Bohn, P. W. *Langmuir* **2007**, *23*, 305–311.
- Fujiwara, T.; Mukose, T.; Yamaoka, T.; Yamane, H.; Sakurai, S.; Kimura, Y. *Macromol. Biosci.* **2001**, *1*, 204–208.
- Kim, M. S.; Seo, K. S.; Khang, G.; Cho, S. H.; Lee, H. B. *J. Polym. Sci., Part A: Polym. Chem.* **2004**, *42*, 5784–5793.
- Tachibana, Y.; Kurisawa, M.; Uyama, H.; Kakuchi, T.; Kobayashi, S. *Chem. Commun.* **2003**, 106–107.
- Shimokuri, T.; Kaneko, T.; Akashi, M. *Macromol. Biosci.* **2006**, *6*, 942–951.
- Wan, A. C.; Mao, H. Q.; Wang, S.; Leong, K. W.; Ong, L. K.; Yu, H. *Biomaterials* **2001**, *22*, 1157–1169.
- Wang, J.; Zhang, P. C.; Lu, H. F.; Ma, N.; Wang, S.; Mao, H. Q.; Leong, K. W. *J. Controlled Release* **2002**, *83*, 157–165.
- Huang, S. W.; Wang, J.; Zhang, P. C.; Mao, H. Q.; Zhuo, R. X.; Leong, K. W. *Biomacromolecules* **2004**, *5*, 306–311.
- Wang, D. A.; Williams, C. G.; Yang, F.; Cher, N.; Lee, H.; Elisseeff, J. H. *Tissue Eng.* **2005**, *11*, 201–213.
- Libiszowski, J.; Kaluzynski, K.; Penczek, S. *J. Polym. Sci., Part A: Polym. Chem.* **1978**, *16*, 1275–1283.
- Pretula, J.; Kaluzynski, K.; Penczek, S. *Macromolecules* **1986**, *19*, 1797–1799.
- Richards, M.; Dahiyat, B. I.; Arm, D. M.; Lin, S.; Leong, K. W. *J. Polym. Sci., Part A: Polym. Chem.* **1991**, *29*, 1157–1165.

- (24) Pretura, J.; Kaluzynski, K.; Szymanski, R.; Penczek, S. *J. Polym. Sci., Part A: Polym. Chem.* **1999**, *37*, 1365–1381.
- (25) Myrex, R. D.; Farmer, B.; Gray, G. M.; Wright, Y.-J.; Dees, J.; Bharara, P. C.; Byrd, H.; Branham, K. E. *Eur. Polym. J.* **2003**, *39*, 1105–1115.
- (26) Wen, J.; Zhuo, R. X. *Macromol. Rapid Commun.* **1998**, *19*, 641–642.
- (27) Renier, M. L.; Kohn, D. H. *J. Biomed. Mater. Res.* **1997**, *34*, 95–104.
- (28) Iwasaki, Y.; Komatsu, S.; Narita, T.; Akiyoshi, K.; Ishihara, K. *Macromol. Biosci.* **2003**, *3*, 238–242.
- (29) Chen, D.-P.; Wang, J. *Macromolecules* **2006**, *39*, 473–475.
- (30) Okuyama, Y.; Yoshida, R.; Sakai, K.; Okano, T.; Sakurai, Y. *J. Biomater. Sci. Polym. Ed.* **1993**, *4*, 545–556.
- (31) Nishida, K.; Yamato, M.; Hayashida, Y.; Watanabe, K.; Yamamoto, K.; Adachi, E.; Nagai, S.; Kikuchi, A.; Maeda, N.; Watanabe, H.; Okano, T.; Tano, Y. *N. Engl. J. Med.* **2004**, *351*, 1187–1196.
- (32) Iwasaki, Y.; Nakagawa, C.; Ohtomi, M.; Ishihara, K.; Akiyoshi, K. *Biomacromolecules* **2004**, *5*, 1110–1115.
- (33) Wachiralarpphaitoon, C.; Iwasaki, Y.; Akiyoshi, K. *Biomaterials* **2007**, *28*, 984–993.
- (34) Iwasaki, Y.; Akiyoshi, K. *Macromolecules* **2004**, *37*, 7637–7642.
- (35) Iwasaki, Y.; Akiyoshi, K. *Biomacromolecules* **2006**, *7*, 1433–1438.

MA0715573

Calcium-Phosphate Formation on Titanium Modified with Newly Developed Calcium-Hydroxide-Slurry Treatment

Naofumi Ohtsu^{1,2}, Tetsuya Ashino¹, Masahito Ishihara¹,
Fuyuki Sakamoto¹ and Takao Hanawa²

¹Institute for Materials Research, Tohoku University, Sendai 980-8577, Japan

²Institute of Biomaterials and Bioengineering, Tokyo Medical and Dental University, Tokyo 101-0062, Japan

Authors developed a new surface-modification method with calcium-hydroxide slurry, which make it possible to treat a titanium surface by contacting with an alkaline agent containing high concentration of calcium. The objective of the new surface modification method was to improve a bone conductivity of titanium with simple and low-cost processes. The calcium-hydroxide slurry was prepared by mixture of calcium-hydroxide reagent and deionized water. A titanium plate was completely buried in the calcium-hydroxide slurry, and the slurry including the titanium was heated in air at 873 K for 7.2 ks, followed by washing in deionized water, and drying in air. Characterization with X-ray photoelectron spectroscopy revealed that chemical state of the surface-modified-titanium surface was the same as that of calcium titanate. X-ray diffraction pattern showed that the perovskite-type calcium titanate was formed in the surface-modified layer, and depth profile by Auger electron spectroscopy titanium indicated that dioxide layer was formed under the calcium-titanate layer. When the surface-modified titanium was immersed in a Hanks' balanced saline solution for 9 d, hydroxyapatite was formed on the surface-modified-titanium surface, while was not formed on the unmodified-titanium surface without surface modification. However, after 18-d immersion, hydroxyapatite was also formed on unmodified-titanium surface. X-ray diffraction pattern showed that thickness of the hydroxyapatite layer formed on the surface-modified-titanium surface was thicker than that on the unmodified-titanium surface. These results indicated that the calcium-hydroxide-slurry treatment improves the performance of calcium-phosphate formation of titanium. Therefore, the new treatment technique is one of the promising methods for improvement of bone conductivity of titanium. [doi:10.2320/matertrans.48.105]

(Received October 13, 2006; Accepted November 22, 2006; Published January 25, 2007)

Keywords: surface modification of titanium, calcium-hydroxide slurry, calcium titanate, calcium-phosphate formation, bone conductivity

1. Introduction

Titanium has been used as biomaterials, such as stem of artificial joints and dental implant, because of its excellent biocompatibility¹⁻⁴⁾ and mechanical strength,⁵⁻⁷⁾ whereas, it takes several months to obtain good fixation between the titanium and bone. Although bulk properties dictate the mechanical properties of biomaterials, tissue-biomaterial processes are surface phenomena and they are governed by surface properties. In order to activate bone conduction, therefore, various surface modification techniques have been attempted. Hydroxyapatite (HAP) coating is the most popular method, and plasma-splaying process is employed for the coating.⁸⁻¹²⁾ With coating of HAP, good biomaterial-bone fixation is obtained.^{10,11)} However, a fracture at the HAP-titanium interface or in the HAP itself is often observed after a long-term use.¹³⁾ Therefore, it can be said that long-term stability of the plasma-sprayed HAP coating is insufficient.

Surface modifications improved the defects of the HAP coating are also studied by some researches. The most important requirement for the improvement is to obtain an unclear interface between the surface-modified layer and titanium substrate, yielding non-destructive interface. Hanawa *et al.* reported that implantation of calcium-ions with an energy of 18 keV modifies titanium surface to be bioactive.^{14,15)} The surface-modified layer of calcium-ion-implanted titanium consists of calcium oxide/hydroxide, titanium oxide, and calcium titanate,^{16,17)} and they concluded that calcium titanate causes of the bioactive surface.¹⁸⁾ Kokubo *et al.* showed that titanium bond to living bone directly if the titanium is treated by soaking in sodium-hydroxide solution

and the subsequent heating.¹⁹⁻²¹⁾ A surface of the treated titanium has sodium-titanate layer with gel-like structure.^{22,23)} After immersed in a simulated body fluid (SBF), sodium in the layer rapidly dissolved in the fluid, calcium in the SBF is taken in the layer instead of sodium, and then, calcium titanate is formed in the treated-titanium surface.^{24,25)} In the above two surface modification methods, calcium titanate is key material for the improvement of bone conductivity.

Recently, some of the authors (N. Ohtsu and T. Hanawa) attempted to improve surface of titanium by calcium-titanate coating with radiofrequency magnetron sputtering.²⁶⁻³⁰⁾ The deposited calcium-titanate layer without some post-treatment has an amorphous structure,^{28,29)} is dissolved in a physiological solution rapidly,²⁷⁾ and is not effective for the improvement.²⁹⁾ Whereas, if successive heating is carried out after the deposition, the calcium-titanate coating is crystallized to be a perovskite structure,^{28,29)} not dissolved easily, and facilitates new bone formation on titanium in hard rat tissue.³⁰⁾ These results indicate that the calcium-titanate coating with perovskite structure modifies titanium surface to be bioactive. However, sputtering technique requires a complex instrument equipped with an ultra-high vacuum system and further is inapplicable to complex-shaped biomaterials. Therefore, the sputtering technique is sometimes not suitable for commercialization, and development of new calcium-titanate coating technique with simple and low-cost is required.

Hanawa *et al.* attempted to form a calcium-titanate on titanium by soaking in a calcium-oxide solution.¹⁸⁾ After soaking in the solution, calcium is taken in the surface, however, the atomic ratio of calcium to titanium (Ca/Ti) is

about 0.1 in the surface,¹⁸⁾ and this ratio much smaller than that of stoichiometric calcium titanate. Hamada *et al.* attempted by hydrothermal modification in calcium-oxide solution.³¹⁾ Although the hydrothermal modification enhances the synthesis of calcium titanate, the atomic ratio of calcium to titanium is still lower than that of stoichiometric calcium titanate, and the calcium-titanate layer is not crystallized to be a perovskite structure. One simple method to increase the concentration of calcium in the modified surface is to treat titanium with an alkaline solution containing high concentration of calcium. However, since the water solubility of calcium oxide and hydroxide is extremely low, it is impossible to prepare the alkaline solution with high calcium concentration.

Authors developed a new surface modification method using calcium-hydroxide slurry. The new method makes it possible to modify titanium surface by contacting with alkaline agent containing high concentration of calcium. The objectives of this study were to characterize a surface of titanium modified with the newly developed calcium-hydroxide-slurry treatment and to estimate performance of calcium-phosphate formation in a SBF. The surface of surface-modified titanium was characterized with grazing incident angle X-ray diffractometry (GI-XRD), X-ray photoelectron spectroscopy (XPS), and depth analysis by Auger electron spectrometry (AES). The surface-modified titanium was immersed in Hanks' balanced saline solution (HBSS), and thereafter, the calcium phosphate formed in the solution were observed with scanning electron microscopy (SEM), and phase of the calcium phosphates were identified with GI-XRD.

2. Experimental Procedures

2.1 Surface modification with calcium-hydroxide-slurry treatment

Commercially available grade 1 pure Ti (cpTi; Furuuchi Chemical Co, Japan) with a disk shape (8 mm in diameter \times 1 mm in thickness), was mechanically polished with SiC paper (#1500) to obtain a rough surface. The titanium plate was soaked in 6 mol L⁻¹ HCl solution at 353 K for 60 s to etch the surface oxide, followed by gently rinsed in deionized water, and dried at 333 K in air. Calcium-hydroxide slurry for the treatment was prepared by a mixture of 1 g of reagent-grade calcium-hydroxide reagent (Nacalai Tesque, Inc) with 1 mL of deionized water (Millipore). Immediately after the mixture, the etched titanium plate was completely buried in the slurry. Then, the slurry containing the titanium plate was heated at 873 K for 7.2 ks in air with an electric furnace. After the heating, the slurry changes to a dry solid with many cracks due to vaporization of water. The titanium plate was retrieved from the slurry, washed ultrasonically in distilled water, and dried at 333 K in air.

2.2 Characterization of surface for the modified-titanium surface.

Chemical state and its composition in the surface were characterized with XPS. The photoelectrons were excited by Al K α radiation ($h\nu = 1486.6$ eV) from a monochromatized X-ray source (SSX-100, Surface Science Inc, U.S.A). The

Table 1 Ion concentrations of Hanks' balanced saline solution (HBSS).

	Concentration (mol L ⁻¹)
Na ⁺	1.42×10^{-1}
K ⁺	5.81×10^{-3}
Mg ⁺	8.11×10^{-4}
Ca ²⁺	1.26×10^{-3}
Cl ⁻	1.45×10^{-1}
HPO ₄ ²⁻	7.78×10^{-4}
SO ₄ ²⁻	8.11×10^{-4}
CO ₃ ²⁻	4.17×10^{-3}

spot size of the X-ray was about 300 \times 500 μ m. The binding energy of Au 4f_{7/2}, Ag 3d_{5/2} and Cu 2p_{3/2} were 84.0, 368.3 and 932.6 eV, respectively and the FWHM of the Au 4f_{7/2} peak was 1.1 eV. Atomic ratio of calcium to titanium (Ca/Ti) was evaluated from the integrated intensities of Ca 2p_{3/2} and Ti 2p_{3/2}, where the sensitive factors installed in the standard SSI software were used for the calculation.

Depth profiles of the elements were determined with AES (JAMP-7100E, JEOL, Japan) with Argon-ion sputtering. The acceleration voltage of electron probe was fixed to 10 kV and that of Ar ions for ion etching was fixed to 3.0 kV. The etching rate estimated with SiO₂ layer was 0.3 nm s⁻¹. The profiles were determined by monitoring of differential spectra for Ti L₃M₂₃M₂₃, Ca L₃M₂M₃, and O KVV transition lines.

Crystallinity of the surface was identified by GI-XRD with a step-scanning mode at 0.8 deg min⁻¹ and the X-ray incident angle $\alpha = 1.0$ degree against the specimen surface (Rotaflex RU-200B, Rigaku, Japan).

2.3 Evaluation of performance for calcium-phosphate formation in HBSS

HBSS was employed as a SBF to evaluate the performance of calcium phosphate formation, whose inorganic contents was similar to that of human blood plasma. The ion concentrations of the HBSS are listed in Table 1. The HBSS was prepared by dissolving prescribed amount of reagent-grade NaCl, KCl, MgSO₄·7H₂O, Na₂HPO₄, KH₂PO₄, and NaHCO₃ (Nacalai Tesque, Inc) in deionized water (Millipore). The pH value of the HBSS immediately after preparation was about 7.4. Four plates of the surface-modified titanium were immersed in 12.6 mL of the HBSS at 310 K. Also, four unmodified-titanium plates, which mechanically polished with SiC paper (#1500), was immersed in HBSS as a control material. Avoiding Si contamination eluted from the vessels,³²⁾ specimens were immersed in the vessels made of perfluoroalkoxy fluoroplastic (Teflon© PFA) and the vessel was completely sealed. In order to avoid the increase of the pH, HBSS were changed once every three days. Two specimens were retrieved from the HBSS after immersion for 9 d; the other two specimens were retrieved after immersion for 18 d. After retrieval, the specimens were gently rinsed with distilled water, and dried at 313 K in air.

Performance for calcium-phosphate formation of the each specimen was estimated by observations of surface using scanning electron microscopy (SEM), where the acceleration voltage of SEM was 10 kV. Phase of the calcium phosphates

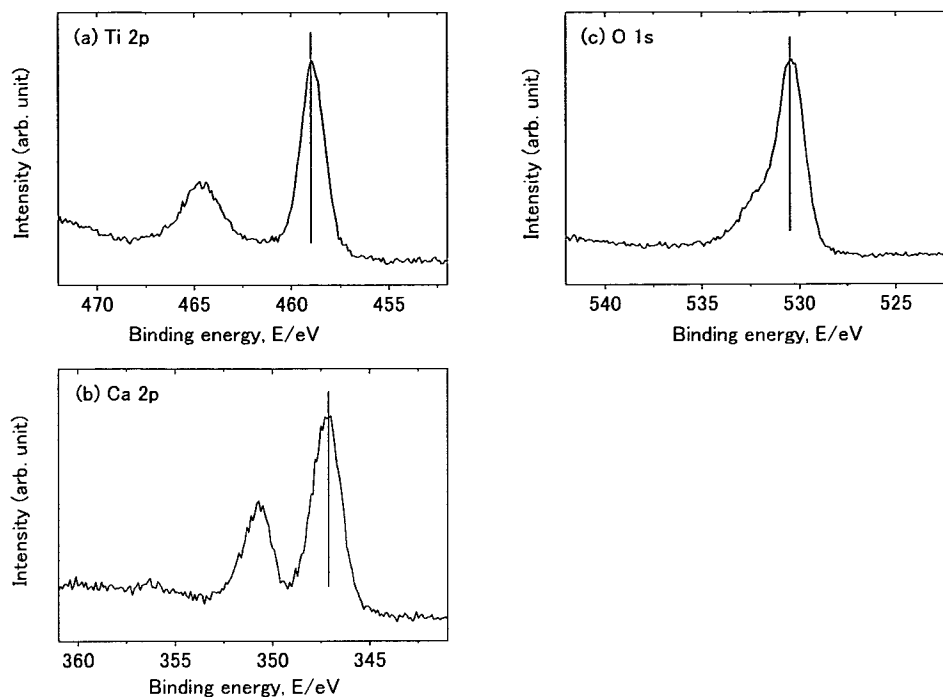


Fig. 1 XPS spectra for the surface-modified-titanium surface: (a) Ti 2p, (b) Ca 2p, and (c) O 1s regions.

were identified with GI-XRD. The measurement conditions of the GI-XRD measurement were the same as the conditions mentioned in the above.

3. Results and Discussions

3.1 Characteristics of the surface-modified-titanium surface

In the XPS survey spectrum for the surface-modified-titanium surface, peaks originated from calcium, titanium, oxygen, and carbon were observed. The binding energy of C 1s peak was 284.8 eV, and origin of carbon was surface contamination adsorbed by exposure to atmosphere. Figures 1(a) and 1(b) show the XPS spectra for Ti 2p and Ca 2p regions, respectively. FWHM of Ti 2p and Ca 2p peaks are 1.4 and 1.8 eV, respectively, and shapes of the peaks are almost symmetry. The results indicate that the chemical states of Ti and Ca consist of one state. Figures 1(c) shows the XPS spectrum for O 1s region. The O 1s peak has small tail in high energy side due to water adsorbed in atmosphere and/or hydroxyl group existing at the outermost surface. It is impossible to estimate which states are dominant in the tail. Binding energies for the modified surface and a calcium titanate of single-crystal are shown in Table 2. The binding energies for the modified surface almost agree with those of the calcium titanate of single-crystal.³³⁾ Furthermore, results of quantitative calculation showed that the atomic ratio of calcium to titanium (Ca/Ti) was 1.0. According to these results, it is concluded that chemical state of the modified surface within the XPS effective depth is calcium titanate.

Depth profile of elements for the modified surface is shown in Fig. 2. The profile of calcium shows that calcium is taken into the surface oxide layer up to ca. 10 nm from the

Table 2 Binding energies of Ti 2p_{3/2}, Ca 2p_{3/2}, and O 1s peaks for the surface-modified-titanium surface and single-crystal calcium titanate.

Electron orbital	Binding energy (eV)	
	Modified surface	Calcium titanate ³²⁾
Ti 2p _{3/2}	459.1	459.1
Ca 2p _{3/2}	347.2	347.3
O 1s	530.5	530.5

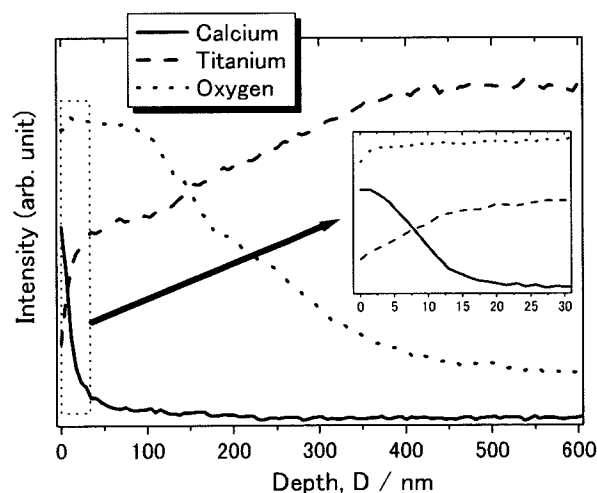


Fig. 2 Depth profile of calcium, titanium, and oxygen for the surface-modified-titanium surface. Inserted figure is enlargement of outermost surface region, which is enclosed by dash line.

outermost surface by the calcium-hydroxide-slurry treatment and the concentration of calcium gradually decreases towards to interior. The profile of oxygen shows that concentration of

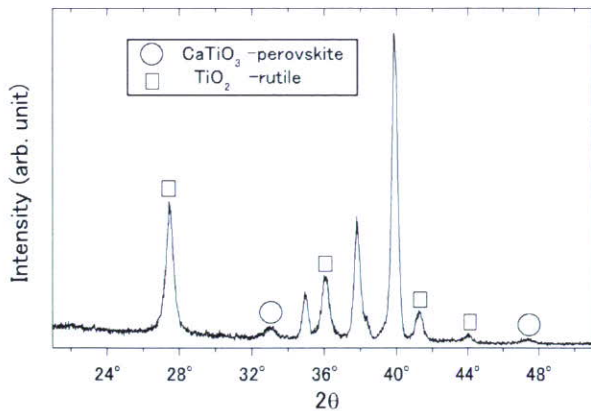


Fig. 3 GI-XRD pattern for the surface-modified-titanium surface.

oxygen diffused into the surface-modified titanium is almost constant up to 120 nm from the outermost surface. Eventually, the surface oxide layer was thickened. The depth range is much larger than that of calcium. These results indicate that surface of the modified titanium has double-layered structure; the outer layer consists of calcium, oxygen, and titanium, and the inner layer consists of oxygen and titanium. Furthermore, in the interface region between the inner layer and titanium substrate, oxygen gradually decreases towards to the substrate. The results indicate that the interface of the modified surface is unclear, that is expected to give non-destructive interface.

Figure 3 shows GI-XRD patterns of the modified surface. Detected peaks except peaks originated from titanium-substrate are identified as those of calcium titanate with perovskite structure and titanium dioxide with rutile structure. It is clear that calcium titanate and titanium dioxide existed at the outer layer and the inner layer, respectively, in the double-layered modified surface.

Some of authors discussed in the previous reports on the characteristics of calcium-titanate film prepared with radio-frequency magnetron sputtering.²⁸⁻³⁰ In the reports, it is concluded that calcium-titanate film which can activate the bone formation should have following two properties: chemical state of calcium is calcium titanate and the film crystallized to be a perovskite-type calcium titanate.^{29,30} Results of the characterization in this study indicated that the calcium-hydroxide-slurry treatment changed titanium surface to the calcium-titanate layer whose characteristics satisfied the requirement for the activation.

3.2 Performance of calcium-phosphate formation in HBSS

SEM images for surfaces of the unmodified and surface-modified titanium after immersion in HBSS for 9 d are shown in Figs. 4(a) and 4(b), respectively. On the surface-modified-titanium surface, many sphere-like precipitates with about 1- μ m diameter are observed. The precipitates are piled up and completely covered the modified surface. On the other hand, no precipitates are observed on the unmodified-titanium surface.

Figure 5 shows the SEM images of the surfaces of the unmodified and surface-modified titanium after immersion in HBSS for 18 d. Also, reduced images are inserted in the upper quarter part of the figures. Both the unmodified and modified surfaces were covered with the precipitate layer. Cracks observed in the layer are due to the evacuation of the water in an ultra-high vacuum. It is clear that the layer formed on the modified surface was thicker than that on the unmodified surface. A part of the layer formed on the modified surface is peeled off. The phenomenon is explained by the effect of stress concentration due to the thick precipitate layer. Peeling off is not observed on the unmodified surface because the layer is not so thick.

Figure 6 shows the GI-XRD patterns for the unmodified-

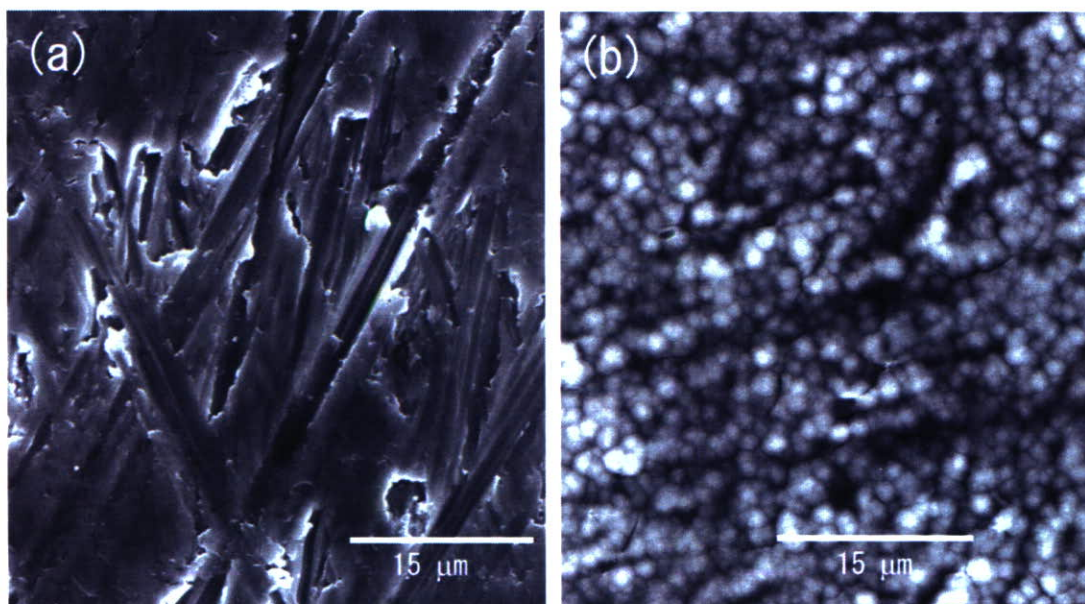


Fig. 4 SEM images for the surface after immersion in HBSS for 9 d: (a) unmodified-titanium surface, and (b) surface-modified-titanium surface.